NTNU – Trondheim
Norwegian University of
Science and Technology

Density Functional Theory Studies of Electronic and Optical Properties of ZnS Alloyed with Mn and Cr

Zenebe Assefa Tsegaye

Condensed Matter Physics
Submission date: June 2012
Supervisor: Jon Andreas Støvneng, IFY

Norwegian University of Science and Technology
Department of Physics

ABSTRACT

This thesis reports the results of first principles theoretical studies of the electronic and optical properties of zinc-blende type ZnS, $Zn_{1-x}Mn_xS$ (x = 1, 0.5, 0.25), and $Zn_{1-x}Cr_xS$ (x = 1, 0.5, 0.25) based on density functional theory (DFT) within the generalized gradient approximation (GGA-PW91) for the exchange-correlation potential. The electronic band structure, total density of states (DOS), partial density of states, and the frequency dependent dielectric function are calculated for the pure and impurity substituted ZnS. The electronic band structure analysis suggests that zinc-blende ZnS is a direct band gap semiconductor. We have also found that the band gap of ZnS is 2.22 eV at Γ point. The ferromagnetic CrS shows a half-metallic behavior with the half metallic gap of 0.32 eV.

We have found half-metallic behavior in Cr impurity substituted ZnS while semiconducting behavior in Mn impurity substituted ZnS. The frequency dependent dielectric function of ZnS, $ZnMnS_2$ and $ZnCrS_2$ is also calculated. The result shows that the static dielectric constant ε_∞ of ZnS is 5.62 and the dielectric function $\varepsilon(\omega)$ is in good agreement with the experimental values. Our results show that the absorption peaks in the low frequency range are not sharp for Mn and Cr impurity substituted ZnS.

Keywords: zinc sulfide, density functional theory, impurity, electronic properties, optical properties

ACKNOWLEDGEMENTS

First of all, I would like to thank the Norwegian government for giving me this chance to study in Norway and for financing my studies as well.

I would like to express my deepest gratitude and thanks to my supervisor Associate professor Jon Andreas Støvneng for his professional guidance and support together with his extraordinary measure of patience, throughout the year.

I would like to extend my heartfelt thanks to my parents for their continuous encouragements and advice.

Last but not least, I am deeply indebted to my friends Teferi Dejene, Gizaw Fikre, Asssefa Derbew, Mamuye Busier, Stephen Nana Akwasi, Feysel Nesru, Zerihun Kinfe, Habte Muluye, Andrea Klubicka, Ashenafi Weldmariam, Webit Kassaye, and Endris Ali for their help and moral support.

Finally, this acknowledgement will not be complete without mentioning the Almighty GOD for his love and mercy.

Zenebe Assefa

June 2012, Trondheim

Norway

TABLE OF CONTENTS

LIST OF SYMBOLS

BZ	Brillouin Zone
CrS	Chromium Sulfide
DFT	Density Functional Theory
DOS	Density of States
FM	Ferromagnetic
GGA	Generalized Gradient Approximation
HM	Half-Metallic
LCAO	Linear Combination of Atomic Orbitals
LDA	Local Density Approximation
MnS	Manganese Sulfide
NAO	Numerical Atomic Orbital
NM	Non-Magnetic
PDOS	Partial Density of States
SCF	Self-Consistent Field
STO	Slater Type Orbital
TDDFT	Time Dependent Density Functional Theory
XC	Exchange and Correlation
ZB	Zinc-blende
ZnS	Zinc Sulfide

LIST OF TABLES

LIST OF FIGURES

1. INTRODUCTION

1.1 Overview

Condensed matter physics is an important input for science and technology. Nowadays it is one of the largest research fields in physics. This field studies material properties from the nano scale to the macroscopic level, experimentally and theoretically.

This master's thesis is a theoretical studies of electronic properties of zinc-blende ZnS, $Zn_{1-x}Mn_xS$ (x = 0.25, 0.5,1), and $Zn_{1-x}Cr_xS$ (x = 0.25, 0.5,1) based on ground state density functional theory (DFT), and optical properties of zinc-blende ZnS, $ZnMnS_2$ and $ZnCrS_2$ based on time dependent density functional theory (TDDFT).

Density functional theory is the most popular and widely used tool for various materials modeling in solid-state physics, chemistry, material physics, and engineering [1]. It is one of the most successful approaches for doing calculations on atoms and molecules. The main idea in DFT calculations is to use the electron density as a basic variable to solve the many body Schrödinger equation. Modern density functional theory was developed by Hohenberg and Kohn in 1964 [2]. The time dependent density functional theory (TDDFT) is an extension of the ground state theory, formulated by Runge and Gross [3] in 1984, which describes the quantum dynamics of electrons induced by a time dependent external potential.

The computational tool used in this master's thesis to study electronic and optical properties is a Fortran based program called Amsterdam density functional (ADF/BAND 2011). The program BAND can be applied to the modeling of chemical and physical properties of periodic structures based on the density functional theory [4] while Amsterdam density functional (ADF) program can be applied to molecules [5].

1.2 Motivation and Objectives

Wide band gap semiconductors, such as ZnS and ZnTe, are attracting vast technological interest because of their potential use at high temperature and strong electric fields in device applications. They are candidate materials in magnetic semiconductor device applications when alloyed with transition metal elements like nickel, chromium, cobalt, and manganese. Half-metallic (HM) ferromagnetism has been a topic of much research interest over the last decades because of its potential in spintronics and applications related to magnetism. The term HM ferromagnetism was first introduced in the work of de Groot et al. [6] in 1983. HM ferromagnetism has been predicted theoretically and experimentally in ferromagnetic metallic oxide CrO_2 [7] and in Cr doped zinc-blende ZnTe diluted magnetic semiconductor (DMS) [8]. The objective of this thesis is to study electronic properties of zinc-blende type ZnS, $Zn_{1-x}Mn_xS$ (x = 0.25, 0.5, 1), and $Zn_{1-x}Cr_xS$ (x = 0.25, 0.5, 1) theoretically based on DFT calculations. The electronic band structure, total density of states (DOS), and partial density of states (PDOS) of these crystals will be investigated. Optical properties of ZnS, $ZnMnS_2$, and ZnCrS2 will also be investigated. The calculation results are compared with available theoretical and experimental values.

1.3 Organization of this work

This work is organized as follows. The report contains six chapters, including the present. The theoretical background of density functional theory and time dependent density functional theory is discussed in chapter 2. Chapter 3 gives a short description of the behavior of electrons in solid state systems and the importance of doping in a semiconductor. This chapter also reviews properties of zinc sulfide.

In chapter 4, computational details will be discussed. Chapter 5 focuses on the results and discussion. In this chapter, calculated results are discussed and compared with other theoretical investigations and experimental results. The summary and recommendations for further work are outlined in chapter 6.

2. THEORETICAL CONSIDERATIONS

In this chapter, a brief review of the theoretical aspects of the project is presented.

2.1 The Schrödinger Equation

Quantum mechanics gives a logically consistent theory of matter on the microscopic level. It can be considered as the basic theory for many areas of science and technology including solid state physics, atomic physics, particle physics, nuclear physics, chemistry, molecular biology, laser devices and so on.

The starting point for any discussion of quantum mechanics is based on the Schrödinger equation [9]. The Schrödinger equation is a differential equation which describes how the wave function Ψ represents a quantum particle's motion under the influence of an external potential V (r). The external potential might be the Coulomb electrostatic potential due to the nuclei of the atoms.

The time independent Schrödinger equation for a quantum particle moving in a three dimensional potential energy field V (r) is given by

$$i\hbar\frac{\partial\Psi(r)}{\partial t}=H\Psi(r), \tag{2. 1}$$

where H is the Hamiltonian operator, which is the sum of a kinetic energy operator and the potential energy of the system. For a single particle of mass m which is moving through space, the Hamiltonian is given by

$$H=\frac{-\hbar^2}{2m}\nabla^2+V(r). \tag{2.2}$$

Here, $\hbar$ is the reduced planck constant. A fundamental postulate of quantum mechanics states that the possible results of a measurement of an observable represented by the operator Q are its eigenvalues q_i only [10, 11, 12]. The eigenvalue equation is given by

$$Q\Psi_i=q_i\Psi_i, \tag{2.3}$$

where Q is an operator and q_i is a number. This is an eigenvalue problem. A solution Ψ of such an equation is called an eigenfunction corresponding to an eigenvalue q_i of the operator Q.

For the time independent Schrödinger equation, the eigenvalue of the Hamiltonian operator is the energy of the system,

$$H\Psi = E\Psi . \tag{2.4}$$

2.1.1 Many Body Systems

Solving the Schrödinger equation for a particular system is important, to understand the behavior of the system, to get information on the density of states of the system, and to understand the response of a particle to an external perturbation [13]. However, the Schrödinger equation has exact solutions for only a few physical problems, such as particle in a box, the simple harmonic oscillator, and the hydrogen atom. For many body systems the Schrödinger equation cannot be solved exactly. Hence, approximation methods are important to solve a many body system's Schrödinger equation [9]. Let us consider a many body system containing N electrons and, in general, several nuclei. We write the full Hamiltonian of this system as

$$H = -\frac{\hbar^2}{2m_e}\sum_i \nabla_i^2 - \sum_{i,I}\frac{Z_I e^2}{r_{i,I}} + \frac{1}{2}\sum_{i\neq j}\frac{e^2}{r_{ij}} - \frac{\hbar^2}{2M_I}\sum_I \nabla_I^2 + \sum_{I,J}\frac{Z_I Z_J e^2}{R_{IJ}} . \tag{2.5}$$

Here, $r_{ij} = \left|\mathbf{r}_i - \mathbf{r}_j\right|$, $R_{IJ} = \left|\mathbf{R}_I - \mathbf{R}_J\right|$, and r_{iI} represents the distance from electron i to nucleus I. The five terms in this equation define, sequentially, the kinetic energy of all the electrons with mass m_e, the interaction potential energy between all electrons and the atomic nuclei, the interaction energy between different electrons, the kinetic energy of all the nuclei with mass M_I, and finally the interaction between the nuclei. Because of the presence of the electron-electron interaction term in the Hamiltonian in (2.5), the Schrödinger equation is not separable. Therefore, approximation methods must be used to solve the many body Schrödinger equation.

The separation of nuclear motion and electronic motion into two mathematical problems is called the Born-Oppenheimer approximation [1]. This approximation method assumes that the motion of the nuclei is so much slower than the motion of the electrons that they can be considered to be stationary. The Born-Oppenheimer approximation allows us to neglect the kinetic energy term of

the nuclei in the Hamiltonian, and the electrostatic repulsion between positively charged nuclei simply represents a constant in the electronic problem. According to the Born-Oppenheimer approximation, the total wave function for the many body system can be written in the following form:

$$\Psi_{\text{total}}\left(\{\mathbf{r}_i\},\{\mathbf{R}_J\}\right)=\Psi_{\text{electon}}\left(\{\mathbf{r}_i\}\right)\Psi_{\text{nuclei}}\left(\{\mathbf{R}_J\}\right). \tag{2.6}$$

Here, $\{\mathbf{r}_i\}$ represents all electron positions; $\{\mathbf{R}_J\}$ represents all nucleus positions. The electronic "clamped-nucleus" Hamiltonian can now be written as

$$H=-\frac{\hbar^2}{2m_e}\sum_i\nabla_i^2-\sum_{i,I}\frac{Z_Ie^2}{r_i}+\frac{1}{2}\sum_{i\neq j}\frac{e^2}{r_{ij}}+\sum_{I,J}\frac{Z_IZ_Je^2}{R_{IJ}}, \tag{2.7}$$

where the last term is the nucleus-nucleus interaction, which has a constant value. Still the present version of the Schrodinger equation is too complex to be solved due to the electron-electron interaction term.

2.1.2 The Hartree-Fock Approximation

The Hartree-Fock approximation is a natural starting point of quantum mechanical calculations for many body systems. The theory approximates the wave function of the many body systems in terms of products of single electron wave function. In this method the total Hamiltonian *H* is sum of single electron Hamiltonian operators H_i. The functional form of the many electron system wave function can be expressed in terms of a single product of single electron wave functions,

$$\Psi\left(\mathbf{r}_1,\mathbf{r}_2,....,\mathbf{r}_N\right)=\chi_1\left(\mathbf{r}_1\right)\chi_2\left(\mathbf{r}_2\right).....\chi_N\left(\mathbf{r}_N\right). \tag{2.8}$$

These single electron wave function are called spin orbitals. Each spin orbital is a product of a special function and a spin state (up and down). This form of Ψ is known as a Hartree product [1]. The Hartree product of spin orbitals has a serious drawback. It does not satisfy the antisymmetry principle, a main criterion for a many fermions wave function. According to quantum mechanics, electrons are fermions, and the antisymmetric principle states that if two electrons are interchanged, the wave function must change sign:

$$\Psi\left(\mathbf{r}_1,\mathbf{r}_2\right)=-\Psi\left(\mathbf{r}_2,\mathbf{r}_1\right). \tag{2.9}$$

The most convenient way to write the wave function of a many electron system is in terms of a Slater determinant of single electron wave functions [1]. The inclusion of a Slater determinant representation of the many electron system into the Hartree theory gives the Hartree-Fock theory.

In a Hartree-Fock calculation, the Coulomb electron-electron interaction potential can be written as

$$V_H(\mathbf{r}) = e^2 \int \frac{n(\mathbf{r}')}{|\mathbf{r}-\mathbf{r}'|} d^3r' . \tag{2.10}$$

The Hamiltonian H corresponding to each electron therefore has a form

$$H = T + V + V_H , \tag{2.11}$$

where V_H (**r**) is the Hartree potential or mean field potential. This is an average Coulomb interaction potential between a single electron and the rest of the electrons in the system. For the N electrons and with spin orbitals, the Slater determinant can be written as

$$\Psi(\mathbf{r}_1, \mathbf{r}_2, .., \mathbf{r}_N) = \frac{1}{\sqrt{N!}} \begin{vmatrix} \chi_1(\mathbf{r}_1) & \chi_1(\mathbf{r}_2) & \cdots & \chi_1(\mathbf{r}_N) \\ \chi_2(\mathbf{r}_1) & \chi_2(\mathbf{r}_2) & \cdots & \chi_2(\mathbf{r}_N) \\ \vdots & \vdots & & \vdots \\ \chi_N(\mathbf{r}_1) & \chi_N(\mathbf{r}_2) & \cdots & \chi_N(\mathbf{r}_N) \end{vmatrix} \tag{2.12}$$

Here, $1/\sqrt{N!}$ is normalization factor. The Slater determinant fulfills the Pauli Exclusion Principle. Exchanging any two rows of a determinant changes the sign of Ψ, which leads to the anti-symmetry principle. If any two rows of a determinant are identical, the determinant will vanish. No two identical electrons occupy the same spin orbitals simultaneously. The Hartree-Fock method gives an exact account of electron exchange [1].

The Hartree-Fock method can be derived from the Rayleigh-Ritz variational method. This Variational method states that for an arbitrary nonzero eigenstate | Ψ >, the expectation value of the Hamiltonian H satisfies the inequality.

$$E_0 = \frac{\langle \Psi | H | \Psi \rangle}{\langle \Psi | \Psi \rangle} \tag{2.13}$$

The energy eigenvalue E_0 is the ground state energy, which is obtained by minimizing the expectation value of the Hamiltonian with respect to a trial wave function.

2.2 Density Functional Theory

In the Hartree-Fock theory, the N electron wave function can be approximated using a single Slater determinant which is a sum of products of wave functions of single electrons. The central idea behind density functional theory (DFT) is to use the electron density as a basic variable, instead of using the many-electron wave function. Density functional theory can be traced back to the works of Thomas and Fermi in the 1920s [14, 15]. The entire field of density functional theory rests upon the two fundamental mathematical theorems proved by Hohenberg and Kohn in 1964 [2] and the Kohn-Sham formulation of density functional theory in 1965 [16].

2.2.1 The Hohenberg-Kohn Theorems

The starting point of any discussion of DFT is the Hohenberg-Kohn theorems [17]. The first theorem states that for any system of interacting particles in an external potential, the ground state electron density, n (**r**), determines the external potential V_{ext} (**r**) fully and uniquely. In other words, there exists a one to one relationship between the electron density and the external potential,

$$n(\mathbf{r}) \rightarrow V_{\text{ext}}(\mathbf{r}) \tag{2.14}$$

According to this theorem, the total energy functional E [n (**r**)] is expressed as

$$E\left[n(\mathbf{r})\right] = \int V_{ext}(\mathbf{r})\, n(\mathbf{r})\, dr + F_{HK}\left[n(\mathbf{r})\right] \tag{2.15}$$

where V_{ext} (**r**) is an external potential (mainly from the nuclei). F_{HK} [n(**r**)] is known as a universal functional, because it does not depend on the external potential. It is the sum of the kinetic energy of the electrons and the contribution from interelectronic interactions. It is given by

$$F_{HK}\left[n(\mathbf{r})\right] = T\left[n(\mathbf{r})\right] + \frac{1}{2}\sum V_H\left[n(\mathbf{r})\right] n(\mathbf{r})\, dr \tag{2.16}$$

The second Hohenberg-Kohn theorem shows that if n (**r**) is normalized to the number of particles in the system, then the total energy of the system E [n (**r**)] becomes a minimum if and only if n (**r**) is the exact ground state density.

2.2.2 The Kohn-Sham Equations

The Hohenberg-Kohn theorems state that the ground state density uniquely determines all ground state observables and it can be determined from the ground state energy functional E [n (**r**)]. However, the theorem does not give us a hint about how to solve the full Schrödinger equation. For example, there is no exact expression for the electron exchange-correlation functional which includes all quantum mechanical effects.

These problems were addressed by Kohn and Sham in 1965 [18]. In the Kohn-Sham scheme, the ground state electron density can be expressed by a set of equations which only involves a system of non-interacting electrons. This non-interacting system has the same electron density n (**r**) as the original system. The energy functional for this system can be given by

$$E\left[n(\mathbf{r})\right] = T_S\left[n(\mathbf{r})\right] + \int V_{\text{eff}}(\mathbf{r})\, n(\mathbf{r})\, d^3r \tag{2.17}$$

The Kohn-Sham equations for electrons moving in an effective external potential can be written as

$$\left[-\frac{\hbar^2}{2m_e}\nabla^2 + V_{\text{KS}}(\mathbf{r})\right]\varphi_i(\mathbf{r}) = \varepsilon_i \varphi_i(\mathbf{r}) \tag{2.18}$$

The solution to this Schrödinger equation yields the Kohn-Sham eigenvalues. The kinetic energy of a system of non-interacting electrons with density $n(\mathbf{r})$ is given b

$$T_{\text{S}}\left[n(\mathbf{r})\right] = \sum_i \left\langle \varphi_i \right| -\frac{\nabla^2}{2} \left| \varphi_i \right\rangle \tag{2.19}$$

where the density of the interacting system is determined by

$$n_s(\mathbf{r}) = \sum_i \left|\varphi_i(\mathbf{r})\right|^2 \tag{2.20}$$

The effective external potential is given by

$$V_{KS}(\mathbf{r}) = V_{\text{ext}}(\mathbf{r}) + V_H(\mathbf{r}) + V_{XC}(\mathbf{r}) \tag{2.21}$$

Here, V_{ext} (**r**) is the Coulomb interaction between an electron and the atomic nuclei, V_H (**r**) is the classical (Hartree) potential describing the Coulomb interaction between the electrons, and V_{XC} (**r**) is the exchange and correlation potential, which describes all the quantum mechanical effects .

The exchange and correlation potential can be formally defined as a functional derivative of the exchange-correlation energy with respect to the electron density,

$$V_{XC}(\mathbf{r}) = \frac{\delta E_{\text{XC}}[n(\mathbf{r})]}{\delta n(\mathbf{r})} \tag{2.22}$$

2.3 The Exchange-Correlation Functionals

The major problem in solving the Kohn-Sham equations is that the true form of the exchange-correlation functional is not known. Two main approximation methods have been implemented to approximate the exchange-correlation functional. The local density approximation (LDA) is the first approach to approximate the exchange-correlation functional in DFT calculations. In this approximation, the local exchange-correlation potential at each position **r** is the exchange-correlation potential for a homogeneous electron gas at the electron density observed at that position [1],

$$V_{XC}^{\text{LDA}}(\mathbf{r}) = V_{XC}^{\text{electron gas}}[n(\mathbf{r})] \tag{2.23}$$

The LDA approximation is exact for a homogeneous electron gas, but the real electron densities are not typically homogeneous over the entire system. The second well known class of approximations to the Kohn-Sham exchange-correlation functional is the generalized gradient approximation (GGA). In the GGA approximation the exchange and correlation energies include the local electron density and the local gradient in the electron density [1],

$$V_{XC}^{\mathrm{GGA}}\left(\mathbf{r}\right)=V_{XC}^{\text{electron gas}}\left[n\left(\mathbf{r}\right)\right] \tag{2.24}$$

2.3.1 Solving The Kohn-Sham Equations

Once we have approximated the exchange-correlation energy, we are in a position to solve the Kohn-Sham equations. The Kohn-Sham equations have an iterative solution; they have to be solved self-consistently. To solve the Kohn-Sham equations for a many body system, we need to define the Hartree potential and the exchange-correlation potential, and to define the Hartree potential and the exchange-correlation potential, we need to know the electron density n (**r**). However, to find the electron density, we must know the single electron wave functions. We do not know these wave functions until we solve the Kohn-Sham equations. The well-known approach to solve the Kohn-Sham equations is to start with an initial trial electron density as illustrated in Figure 2.1. Then solve these equations using the trial electron density.

After solving the Kohn-Sham equations, we will have a set of single electron wave functions. Using these wave functions, we can calculate the new electron density. The new electron density is an input for the next cycle. Finally, compare the difference between the calculated electron densities for consecutive iterations. If the difference in electron density between consecutive iterations is lower than an appropriately chosen convergence criterion, then the solution of the Kohn-Sham equations is said to be self-consistent. Now the calculated electron density is considered as the ground state electron density, and it can be used to calculate the total energy of the system [1].

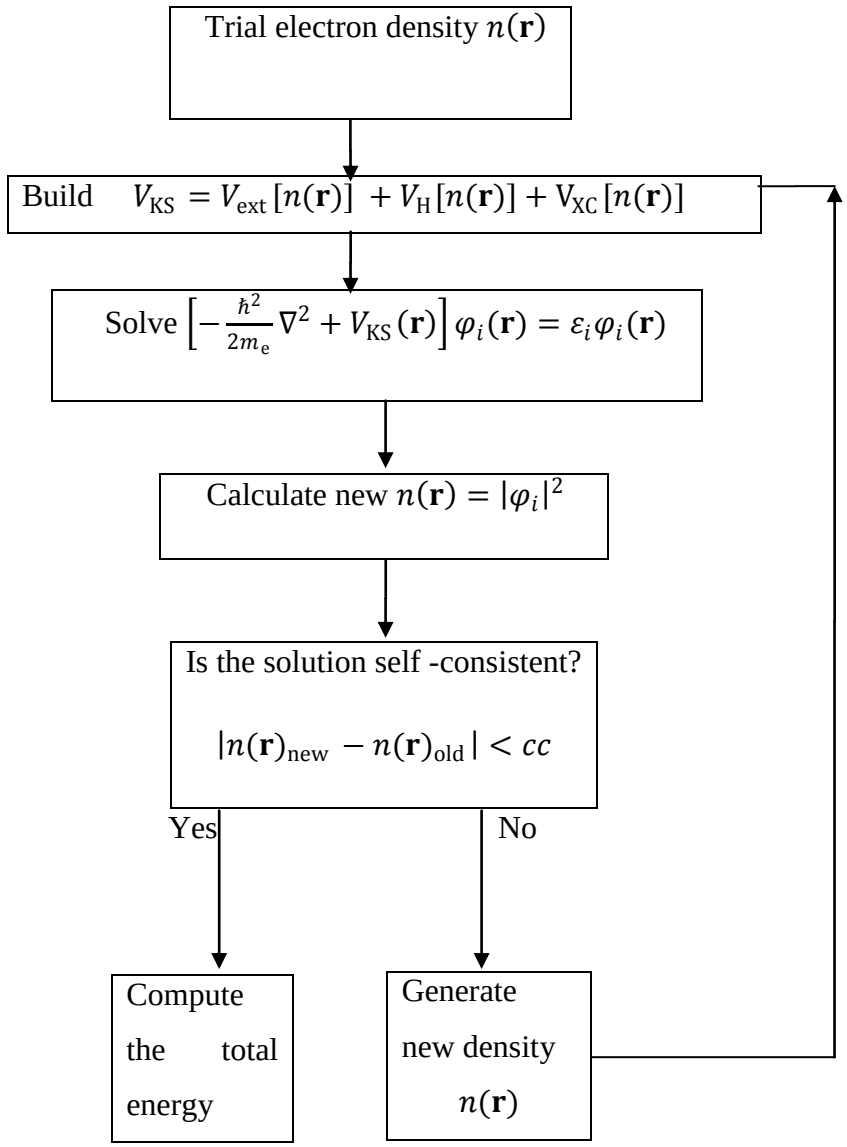

Figure1.1: Illustration of the self-consistent field (SCF) procedure for solving the Kohn-sham equations where cc is an appropriately chosen convergence criterion.

2.4 Time Dependent Density Functional Theory (TDDFT)

The time dependent density functional theory has been proposed as a tool to describe the quantum dynamics of electrons induced by a time dependent external potential [3]. It was first formulated by Runge and Gross [19] in 1984. TDDFT is an extension of ground state density functional theory, deals with excited states of the system, and time dependent processes such as electronic excitation spectrum and frequency dependent dielectric response of crystalline solids.

2.4.1 The Time Dependent Hohenberg-Kohn Equations

The analogy of the Hohenberg-Kohn theorems for time dependent systems is the Runge-Gross theorem [17]. The Runge-Gross theorem states that for a given initial state at time t_0 there is a one-to-one correspondence between the time-dependent external potential V_{ext} (**r**) of the system and its time dependent density *n* (**r**).

The non-relativistic time dependent Schrödinger equation for the interacting many particle system takes the form

$$i\frac{\partial}{\partial t}\Psi\left(\{\mathbf{r}\},t\right)=H\left(\{\mathbf{r}\},t\right)\Psi\left(\{\mathbf{r}\},t\right) \tag{2.25}$$

The Hamiltonian of the time dependent system of interacting particles is *H* (t). If we solve the time-dependent Schrödinger equation for a fixed initial state at t_0 and several external potentials V_{ext}(**r**, t), we obtain a one-to-one correspondence between the external potential and the density,

$$V_{ext}\left(\mathbf{r},t\right)\rightarrow\Psi\left(t\right)\rightarrow n\left(\mathbf{r},t\right) \tag{2.26}$$

2.4.2 The Time Dependent Kohn-Sham Equations

The time dependent density *n* (**r**, t) of the interacting system can be calculated as the density n_s (**r**, t) an auxiliary non-interacting system of electrons. For an interacting electron system with external potential *V* (**r**, t), a Kohn-Sham potential exists such that the density n_s(**r**, t) of the non-interacting system equals the density *n* (**r**, t) of the interacting system [3].

The time-dependent electron density n (**r**, t) is given by

$$n(\mathbf{r},t) = n_s(\mathbf{r},t) = \sum_{i=1} \left|\varphi_i(\mathbf{r},t)\right|^2 \tag{2.27}$$

Hence, the time-dependent Kohn-Sham wave functions are obtained by solving the time dependent Schrödinger equation of the non-interacting electrons,

$$i\frac{\partial}{\partial t}\varphi_i(\mathbf{r},t) = \left[-\frac{1}{2}\nabla^2 + V_{KS}[n](\mathbf{r},t)\right]\varphi_i(\mathbf{r},t) \tag{2.28}$$

The single particle Kohn-Sham potential is given by

$$V_{KS}[n](\mathbf{r},t) = V_{ext}(\mathbf{r},t) + V_H[n](\mathbf{r},t) + V_{XC}[n](\mathbf{r},t) \tag{2.29}$$

Here, the first term is external potential, is the Hartree potential, and is the exchange-correlation potential. The exchange-correlation potential can be defined as a functional derivative of an exchange-correlation energy with respect to the time-dependent density at a particular time t.

2.5 Dielectric Response

Insulating materials show a very interesting dielectric response to an externally applied electric field due to the absence of mobile charges. The response of non-conducting dielectrics to an externally applied electric field is called polarization.

The theory of the dielectric properties of solids describes the response of non-conducting crystals to externally applied electric fields [3]. The induced field opposes the externally applied field and reduces the perturbing field inside the solid.

Consider a periodic crystal system, subject to an external applied electric field $\mathbf{E}_{\text{mac}}(\mathbf{r}, t)$. This field causes charges in the solid to displace, and experience induced macroscopic polarization $\mathbf{P}_{\text{mac}}(\mathbf{r}, t)$, which can be written as

$$\mathbf{P}_{mac}(\mathbf{r},t) = \int_{t_0}^{t} \chi_e(t-t').\mathbf{E}_{mac}(\mathbf{r},t')dt' \tag{2.30}$$

Here, χ_e (t) is the dielectric susceptibility of the material, which is used to calculate the dielectric function.

The macroscopic electric field $\mathbf{E}_{mac}(\mathbf{r}, t)$ is the average of the external applied field plus the induced field. Thus, polarization is the response of the system to the externally applied electric field and the induced field [3]. In the time dependent density functional theory a crystalline system is modeled via a lattice periodic microscopic scalar potential with a time dependent external electric field as a perturbation force [20].

This microscopic Coulomb potential is due to the induced density. Thus, the electron dynamics is described by the time dependent Kohn-Sham equations,

$$i\frac{\partial}{\partial t}\Psi_n(\mathbf{r},t)=\left(\frac{1}{2}\left|-\nabla+\frac{1}{c}\mathbf{A}_{eff}(\mathbf{r},t)\right|^2+V_{eff}(\mathbf{r},t)\Psi_n(\mathbf{r},t)\right) \tag{2.31}$$

where V_{eff} (**r**, t) is the time dependent effective potential, which is the sum of the Coulomb and exchange-correlation contributions of the perturbed density, and $\mathbf{A}_{\text{mac}}$ (**r**, t) is the externally applied vector potential, which is obtained by replacing the ground state momentum operator by

$$p=-i\nabla+\frac{1}{c}\mathbf{A}_{eff}(\mathbf{r},t) \tag{2.32}$$

The time dependent density functional theory equations have an iterative solution, in which the macroscopic electric field is kept constant and the microscopic potential is updated in each cycle, until a self-consistent solution is reached [21].

2.5.1 Dielectric constant

Optical constants are quantities used to describe the optical properties of a material [22]. The responses of periodic systems to a spatially uniform externally applied electric field are described by a complex dielectric function according to

$$\varepsilon(\omega)=\varepsilon_1(\omega)+\varepsilon_2(\omega) \tag{2.33}$$

The imaginary part of the dielectric function, $\varepsilon_2(\omega)$, is closely related to the absorption spectra [23, 24].

In cubic lattice structures, the *x*, *y*, and *z* axes are indistinguishable. Hence, optical properties are isotropic, i.e., $\varepsilon_{xx} = \varepsilon_{yy} = \varepsilon_{zz}$ in cubic crystals.

The imaginary part of the dielectric function for transitions between the valence band *i* and the conduction band *j* can in the small frequency range be derived from an electronic structure calculation, using the dipole matrix element, $M_{ij}(k)$ and an energy conserving delta function,

$$\varepsilon_2(\omega) = \frac{e^2\hbar}{\pi m^2 \omega^2} \sum_{i,j} \int_{BZ} \left| M_{ij}(k) \right|^2 \delta\left[\omega_{ij}(k) - \omega \right] d^3k \tag{2.34}$$

where the dipole matrix element is given by

$$M_{ij}(k) = \left\langle \left| u_i(k) \right| \nabla \left| u_j(k) \right| \right\rangle \tag{2.35}$$

Here, $u_i(k)$ and $u_j(k)$ are the periodic parts of the Bloch wave functions [25]. The real part of $\varepsilon(\omega)$ can be derived from the imaginary part using the Kramers-Kronig relations,

$$\varepsilon_1(\omega) = 1 + \frac{2}{\pi} P \int_0^{\infty} \frac{\omega' \varepsilon_2}{\omega'^2 - \omega^2} d\omega' \tag{2.36}$$

where *P* denotes the principal value of the integral.

3. ELECTRONS IN SOLID STATE SYSTEMS

3.1 Electronic Band Structure

Based on the arrangement of atoms in solids, we can categorize solid state materials into crystalline and amorphous materials. Crystalline solids are well-known by the fact that atoms making up the crystal are arranged in a periodic manner.

Due to the variation in electronic band structure, a wide range of electrical and optical properties are observed in solid state materials. The electronic band structure of each solid material is unique. As the atoms in solid state material packed closer together with the interatomic separation distance to form a solid, their outer orbitals overlap and interact strongly with each other and as a result electronic bands are formed [22].

3.1.1 Bloch's Theorem

It is difficult to calculate the wave function for each of the interacting electrons which extend over the total space of the solid. Bloch solved this problem by using symmetry properties of the crystals. Bloch's theorem uses the periodicity of a crystal to calculate the wave function of electrons in the unit cell of a crystal [22, 25].

Atoms in a crystalline material are arranged in a periodic manner. Hence, the external potential for an electron in the crystal is also periodic, with periodicity the same as the length *l* of the unit cell of the crystal. A periodic potential is a precondition for Bloch's theorem and can be expressed as

$$V(\mathbf{r}) = V(\mathbf{r} + l) \tag{3.1}$$

Bloch's theorem states that the electronic wave functions for a periodic potential must be expressed as the product of a plane wave and an envelope function that has the periodicity of the crystal lattice [22]. For the wave vector **k** the Bloch function takes the form

$$\Psi_k(\mathbf{r}) = u_k(\mathbf{r}) e^{i\mathbf{k}.r} \tag{3.2}$$

Consider a simple three dimensional lattice where the positions of the atoms in real space are defined by the lattice vectors $\mathbf{a}_1$, $\mathbf{a}_2$, and $\mathbf{a}_3$ the real space positions $\mathbf{R}$ can be written as

$$\mathbf{R} = u\mathbf{a}_1 + v\mathbf{a}_2 + w\mathbf{a}_3 \tag{3.3}$$

where *u*, *v*, and *w* are integers. For a simple cubic lattice, the real space lattice vectors have

$$|a_j| = a \qquad \text{for all j.} \tag{3.4}$$

High symmetry points within the first Brillouin zone of the reciprocal space (or simply *k*-space) is given unique names derived from irreducible representations of point group theory [26]. The Γ point at k = (0, 0, 0) is the point at the origin of the Brillouin zone. The X point at k = $2\pi/a$ (1, 0, 0) is the centre of square face at the surface of the Brillouin zone. The L point at k = π/a (1, 1, 1) is the center of the hexagonal face at the surface of the Brillouin zone.

Δ is an arbitrary point between Γ and X, whereas an arbitrary point between Γ and L is labeled Λ. The first Brillouin zone encloses the part of *k* space from $-\pi/a$ to π/a (in one dimension). The second Brillouin zone encloses the part of *k* space between $\pi/a \rightarrow 2\pi/a$, and $-\pi/a \rightarrow -2\pi/a$.

3.2 The Density of States

The density of states (DOS) is a quantity used to describe the electronic states of a solid. The concept of the density of states is the result of the electronic band formation in solids [22]. The density of states is defined as the number of electronic states or unit energy within a given energy interval. It is conveniently expressed in terms of the density of states function *D* (ε), which can be written in the form

$$D(\varepsilon) = \sum_i \delta(\varepsilon - \varepsilon_i) \tag{3.5}$$

Here, the sum runs over all Kohn-Sham eigenvalues ε_i (k). The local DOS is can be defined as the number of electronic states at a specified energy in a volume around an atom [1]. We can now redefine the total DOS as the sum of the local density of states of all atoms in a crystal,

$$D(\varepsilon) = \sum_n d_n(\varepsilon) \tag{3.6}$$

Here, n represents different atoms of the unit cell and d_n (ε) is the local density of states. A decomposition of the local states into state-resolved density of states corresponds to the projected density of states (PDOS).

The density of states of a perfect crystal is zero in the band gap because there are no allowed energy levels in the band gap E_g. In crystalline solids, the band gap differentiates the valence and the conduction bands as shown in Figure 3.1.

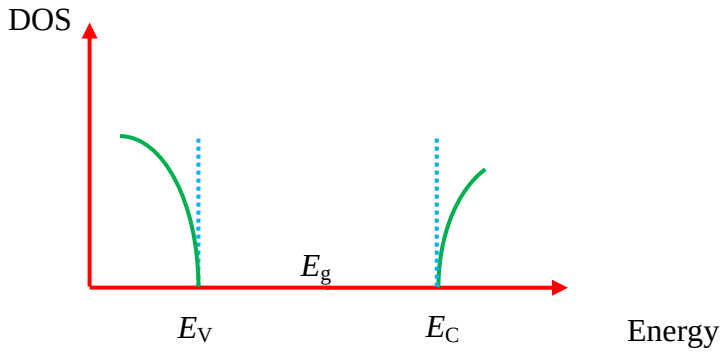

Figure 3.1: Electronic DOS of crystalline solids near the band gap. The DOS can be divided into two separate regions, the valence and the conduction bands.

The amorphous materials may possess short-range order, but they lack long range order. In amorphous materials, electronic states are not described by Bloch's theorem rather than can be separated into extended states and localized states. The extended states are separated from the localized states by mobility edges as shown in Figure 3.2. In amorphous materials, energy difference between the valence band mobility edge E_μ^V and the conduction band mobility edge E_μ^c is called the mobility gap [13].

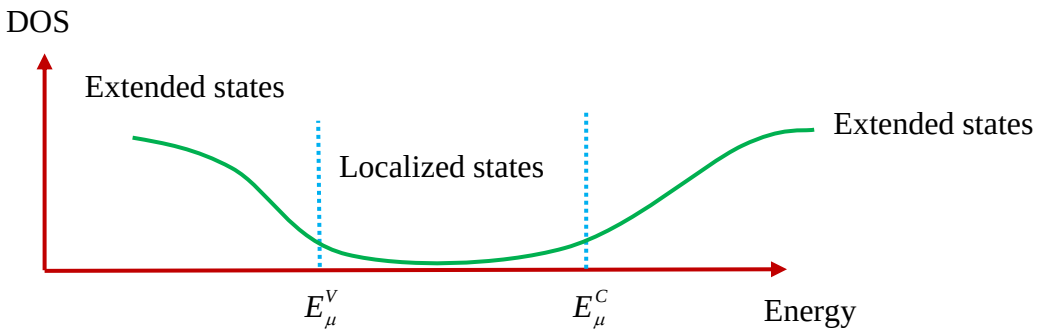

Figure 3.2: Electronic DOS of amorphous materials.

3.3 Doping of Semiconductors

The intrinsic carrier density has little use in semiconductor devices [13]. The process of adding impurities into the crystal lattice of a pure (intrinsic) semiconductor at a very low level is known as doping. The added impurity atom is called dopant atom and its presence in the crystal can considerably change the electrical and optical properties of the material. A doped semiconductor is called an extrinsic semiconductor. In general, we can use the term impurity states to describe localized electronic states of the crystal which are due to an impurity replacing one atom of the lattice [26, 27].

There are two kinds of extrinsic semiconductor: n-type semiconductor and p-type semiconductor. An n-type semiconductor is formed by adding pentavalent impurity into a pure group IV semiconductor. The introduction of donor atoms from group V of the periodic table like P, As, and Sb into Si or Ge creates an excess of electrons. The donor atoms shift the Fermi level, break the translational periodicity of the crystal, and introduce a new energy level called a donor level E_d near the edge of the conduction band in the energy band structure within the band gap of the intrinsic semiconductor as shown in Figure 3.3.

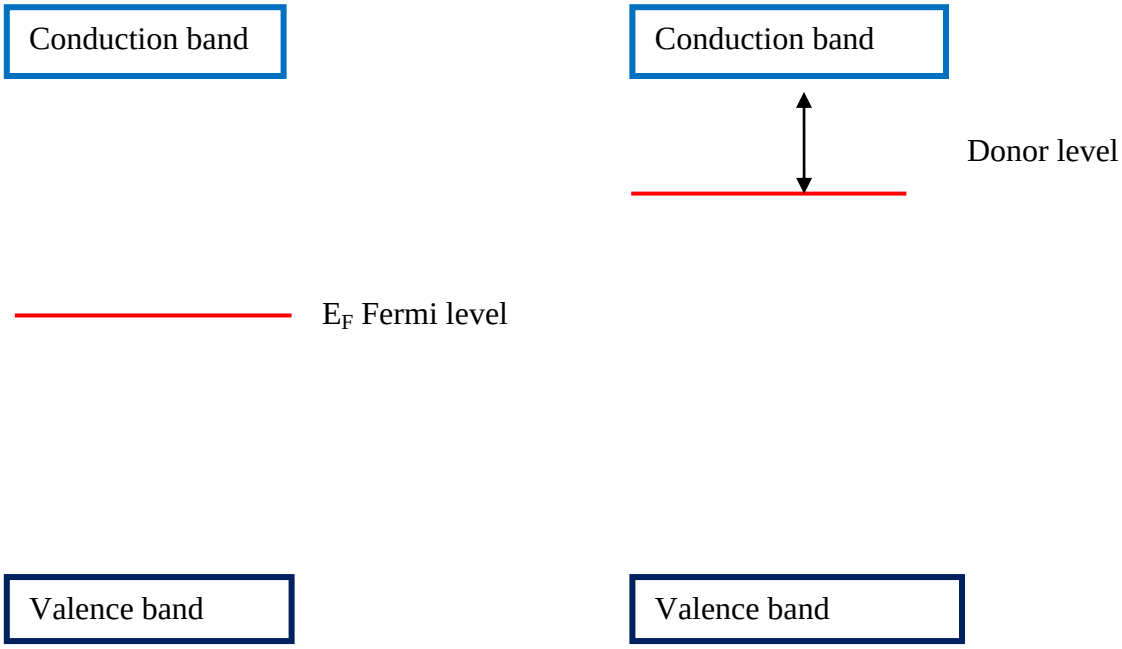

Figure 3.3: Electronic band diagram of a) an intrinsic semiconductor, and b) an n-type semiconductor. In b) a donor level is produced below the conduction band edge.

A p-type semiconductor is formed by doping a pure group IV crystal with impurity atoms from group III of the periodic table. This intentional introduction of acceptor impurities into the crystal during crystal growth leads to a deficit of electrons and thus creates an excess of holes. The impurity atoms that can accept electrons from the valence band, creating holes, are called acceptor atoms. The acceptor atom creates a new energy level just above the top of the valance band within the band gap as shown in Figure 3.4.

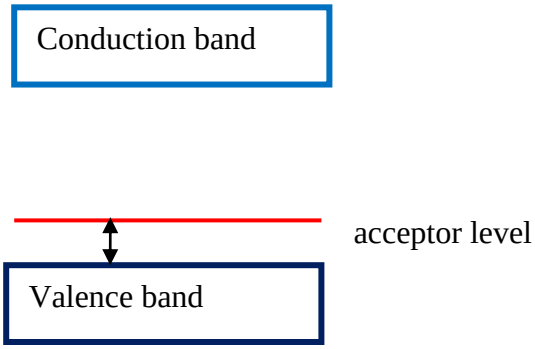

Figure 3.4: Electronic band diagram of p-type semiconductor. An acceptor level is produced above the top of the valence band. At room temperature, electrons can easily be excited from the valence band to

3.4 Properties of ZnS

Wide band gap semiconductor materials, such as ZnS and ZnTe, are attracting vast technological interest because of their potential use in device applications at high temperature and strong electric fields [13]. ZnS is an important II-VI compound semiconductor. With a direct, band gap energy of 3.8 eV [28] at room temperature; it has a potential application in optoelectronic devices, thin film solar cells and electroluminescent devices. ZnS exists in two different crystal structures; that of cubic zinc-blende and that of hexagonal wurtzite structure. In the cubic crystal structure of ZnS, the *x*, *y*, and *z* axes are identical, and their optical properties are isotropic [22].

3.5 Optical Properties

Solid-state materials show wide range of optical properties. Interband transition, excitonic absorption, and impurity absorption are some of the electronic band processes contributes to the optical properties of solids.

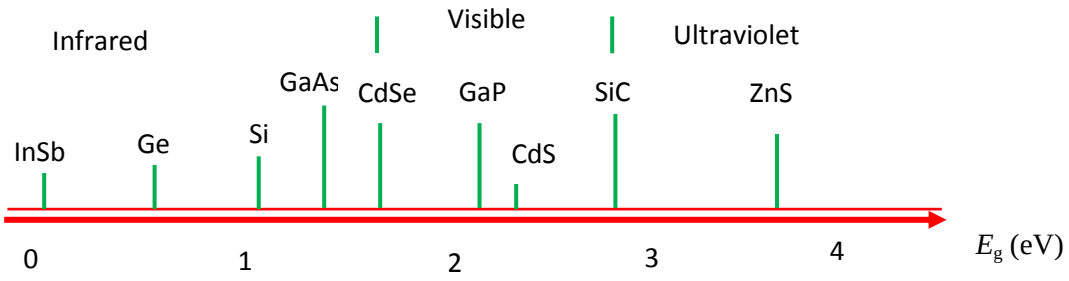

Figure 3.5: Band gap of some common semiconductors relative to the optical spectrum.

3.5.1 Interband Transition

Semiconductors and insulators absorb photons in the infrared, visible, or ultraviolet spectral regions. In a pure semiconductor, only a photon with energy greater than the band gap energy E_g is able to excite an electron from the valence band to the empty conduction band. The process in which an electron jumps from the band at lower energy to the one above it by absorbing a photon is called an interband transition [22, 29]. Figure 3.6 shows the interband absorption between initial E_i and final E_f states of energy.

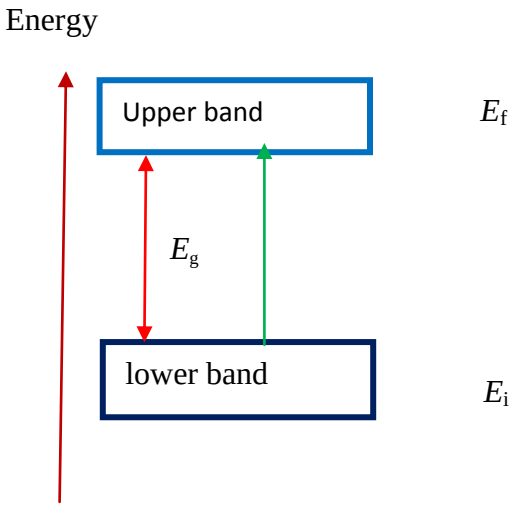

Figure 3.6: Interband optical absorption between an occupied valence band and an empty conduction band.

where E_g is the minimum energy difference between the top of the valence band and the bottom of the conduction band, E_i is the energy of an electron in the filled lower band, and E_f is the

energy of an electron in the upper empty band. Hence, by using the law of energy conservation E_f can be written as

$$E_f = E_i + \hbar\omega \tag{3.7}$$

Here, $\hbar\omega$ is the energy of the photon. The interband transitions will be possible over a continuous range of frequencies, because there is a continuous range of energy between the upper and lower bands [22]. It can also correspond to the creation of an electron-hole pair (EHP).

3.6 Direct and Indirect Gap Materials

The interband absorption rate depends on the band structure of the semiconductor. The band structure or *E* (k) diagram of a semiconductor is a plot of the total energy of an electron as a function of electron wave vector within some region of the Brillouin zone. We have two types of semiconductor band gap; direct and indirect [13, 22]. Figure 3.7 shows the *E* (k) diagram of a direct and an indirect band gap material.

In a direct gap semiconductor, the valence band maximum and conduction band minimum occur at the zone center where **k** = 0. Hence, there is no net transfer of momentum associated with the interband transition in a direct band gap semiconductor. If the valence band maximum and conduction band minimum do not occur at **k** =0 in *k* space, then an interband transition must involve a phonon to conserve momentum, and the material is called an indirect gap semiconductor.

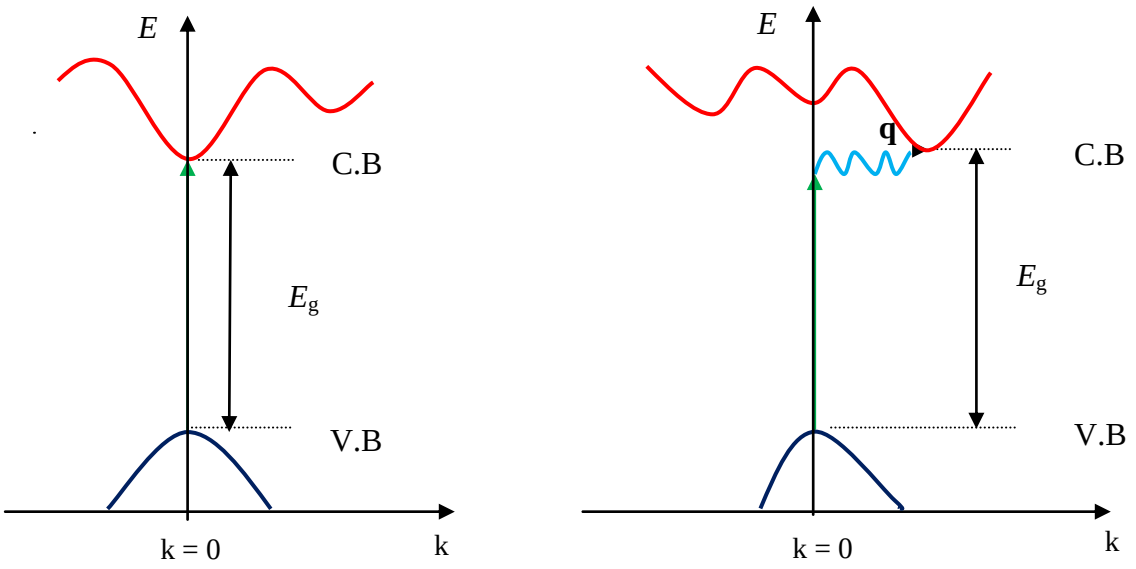

Figure 3.7: Interband transition in a) direct band gap; b) indirect band gap materials.

Conservation of energy and momentum for an indirect transition can be expressed as follows

$$E_f = E_i + \hbar\omega + \hbar\Omega \tag{3.8}$$

$$\hbar\mathbf{k}_f = \hbar\mathbf{k}_i + \hbar\mathbf{q} \tag{3.9}$$

Here, Ω is the energy of a phonon with wave vector **q**, (E_i, $\mathbf{k}_i$) is an electron in the valence band state, and (E_f, $\mathbf{k}_f$) is an electron in the conduction band state.

An optical property of solids is directly related to the nature of electronic band structure. For example, in the direct gap semiconductor, the optical transitions are very strong [13, 29]. In Contrast, in an indirect gap material, the transition must involve a phonon to conserve momentum. This decreases the transition rate for exciting an electron from the valence to the conduction band by absorption of a photon of angular frequency ω. Direct gap materials can be used for high performance optoelectronic devices. In this project, we focus on the direct gap material ZnS, which is ideal for studying optical phenomena.

3.7 Excitons Absorption

In semiconductors or insulators, the absorption of a photon creates a hole in the valence band and an electron in the conduction band [26]. The Coulomb interaction between the hole in the valence band and the electron in the conduction band can create bound electron-hole pair called an exciton. Excitons allow a semiconductor to absorb photons with less energy than the band gap because it has a lower energy than an unbound electron-hole pair.

The two types of excitons observed in many crystalline materials are: the free and the tightly bound excitons. The free excitons are weakly bound electron-hole pairs and they can move freely throughout the semiconductor. They are mainly observed in semiconductors. The tightly bound excitons are localized states and observed in insulators [22]. Formation of excitons is not common in doped semiconductors. As we discussed earlier, impurities introduce unpaired free electrons and holes into the semiconductor. These unpaired free carriers strongly reduce the binding forces and screen the Coulomb interaction in the excitons [22].

3.8 Impurity Absorption

Impurity states have sharp features in the density of states plot near the valence band maximum for acceptor atoms or, near the conduction band minimum for donor atoms. If there is a large impurity concentration, these states can extend into impurity bands. These newly introduced impurity states give rise to two new absorption mechanisms as shown in Figures 3.8 and 3.9 below.

- In an n-type semiconductor, if the donor levels are occupied, transitions will be possible between donor levels by absorbing photons with energy less than the band gap.

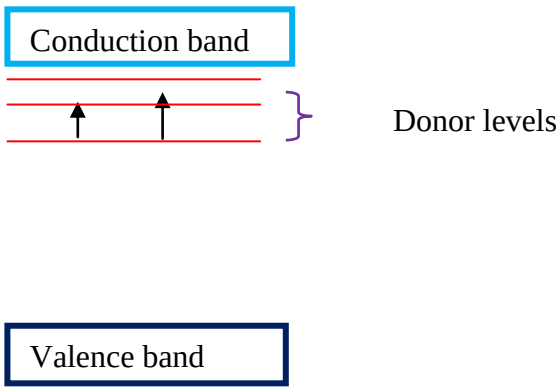

Figure 3.8: Absorption in an n-type material: transition between donor levels.

- In a p-type semiconductor, if the acceptor levels are empty, transitions will be possible from the valence band to empty acceptor levels by absorbing photons with energy less than the band gap.

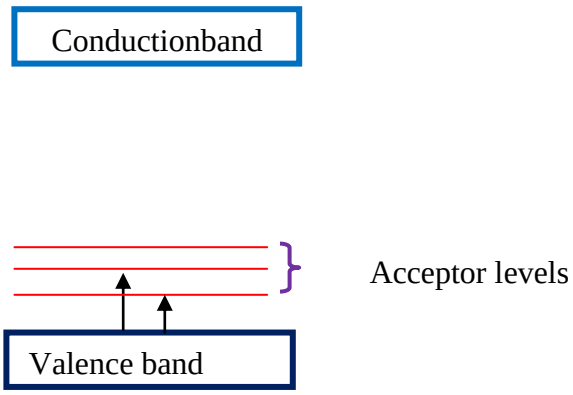

Figure 3.9: Impurity absorption in a p-type material: transition from the valence band to empty acceptor levels.

3.9 Luminescence

Luminescence is the property of light emission by the material. In semiconductors, the interband luminescence occurs when excited electrons in the conduction band drop down to the valence band by the emission of photons. There are three important excitation mechanisms [22].

- Photoluminescence: the emission of light from a semiconductor after absorbing a photon.
- Electroluminescence: the emission of light caused by the introduction of electric current into the material.
- Cathodoluminescence: the emission of light caused by the bombardment of the sample by high-energy electrons.

4. COMPUTATIONAL DETAILS

In this project work, electronic and optical properties of zinc-blende type ZnS, $Zn_{1-x}Mn_xS$ (x = 1, 0.5, 0.25), and $Zn_{1-x}Cr_xS$ (x = 1, 0.5, 0.25) are studied based on the quantum mechanical modeling method density functional theory (DFT). The calculations were performed using the program Amsterdam density functional (ADF/BAND). This program calculates single electron Kohn-Sham wave functions self-consistently within the framework of DFT. For the treatment of electron exchange and correlation energies, we used Perdew-Wang (PW91) [30] within the generalized gradient approximation.

The periodic program BAND evaluates various integrals in k space within the Brillouin zone using tetrahedron method [4, 31]. We used KSPACE parameter equal to 7 for structural optimization and calculation of electronic properties of all compounds, while KSPACE = 5 was used to calculate optical properties of ZnS, $ZnMnS_2$, and $ZnCrS_2$. BAND uses Slater-type atomic orbitals (STO_s) to approximate the Bloch wave functions of the core electrons and the valence electrons [4]. We also employed a triple zeta basis, augmented with two polarization functions (TZ2P). Relativistic corrections are not included in the calculations.

All geometries in this work are minimum energy geometries. We start with an initial geometry. Then the periodic program BAND calculates all the forces on the atoms self consistently until a convergence criterion is reached. Self-consistency has been achieved by allowing the total energy to converge within 0.001eV.

To study the effects of introducing Mn and Cr impurities on electronic structure and optical properties of ZnS computationally large super cells are required both to compare with experimental doping fractions and to minimize dopant-dopant interactions. However, modeling of large super cells is computationally expensive.

In this project, due to time limitation, we chose to look at small unit cells, up to 8 atoms, to obtain a first idea about how the impurities affect the electrical and optical properties of ZnS. We used the small frozen core approximation for ZnS, and the medium frozen core option for $ZnMnS_2$ and $ZnCrS_2$ to study the effect of impurity on optical properties. The dielectric

functions are calculated in the spectral range 0 - 14 eV using periodic program BAND within the framework of time dependent density functional theory. We used GGA-PW91 for the treatment of electron exchange and correlation energy, and TZ2P basis set.

4.1 k-Point Sampling

For a periodic system the solution to the Schrödinger equation must satisfy the fundamental property of Bloch's theorem. The electronic wave functions for energy band *i* and wave vector **k** have the form:

$$\Psi_{i,k}(\mathbf{r}) = u_{i,k}(\mathbf{r}) e^{i\mathbf{k}\cdot r} \tag{4.1}$$

The first Brillouin zone can be defined as a primitive cell in *k* space. It plays an essential role in the electronic band theory of materials.

Two widely used methods of choosing *k* points to sample Brillouin zone precisely are Monkhorst-Pack [32] and tetrahedral methods [33]. The Brillouin zone is divided into an equally spaced grid of *k* points in the Monkhorst-Pack scheme, whereas in the tetrahedral methods it is divided into tetrahedral volumes not essentially equivalent in three dimensions.

A symmetry operation of the crystal reduces integrations in *k* space. A highly symmetric crystal such as a face-centered cubic crystal requires only a small number of distinct points in *k* space. The irreducible Brillouin zone (IBZ) is the reduced region in *k* space by the symmetry operations of the lattice [1].

4.2 Basis Set

The atomic orbials are obtained from the expansion of a set of functions called the basis set. There are different types of basis set such as, Gaussian type and Slater- type functions. Slater-type orbitals have been used frequently for the expansion of the electron wave functions, in contrast to the Gaussian-type orbitals (GAO_s). The Slater type orbitals have an exponential nature and are the most commonly used basis function in quantum mechanical calculations [34].

The BAND program includes a database of Slater type orbitals basis set with increasing size and accuracy are the single-zeta basis set (SZ), double-zeta (DZ), and double-zeta augmented with polarization function (DZP), TZ2P basis sets.

5. RESULTS AND DISCUSSION

In this part of the project results of the calculations are presented. First, structural and electronic properties of zinc-blende ZnS, MnS, and CrS are discussed. Second, effects of incorporation of Mn and Cr impurities on the electronic structure are presented, followed by optical properties of ZnS. The optical properties of some doped structures are also compared with that of pure ZnS.

5.1 Structural Properties

In Table 5.1, we provide a comparison of LDA and GGA band gaps for ZnS. It is a fact that DFT within the local density approximation (LDA) or the generalized gradient approximation (GGA) correctly predicts the existence of a band gap for semiconductors and insulators. However, the magnitude of this gap is not predicted accurately. The underestimation of the band gap is mainly due to the fact that the exact functional introduced in the Hohenberg-Kohn theorem is not known.

Table 5.1: Band gaps for the zinc-blende crystal structure of ZnS calculated at the experimental value of the lattice constant a =5.41 **Å** [28].

Solid	Method	E_g(eV)
ZnS	LDA(This work)	1.985
	GGA(This work)	2.143
	Expt.	3.80[a]

[a]Reference 28.

The results show that the GGA-PW91 calculations predict a lattice constant of 5.47 Å, which overestimates the experimental value of 5.41 Å by about 6%.

As part of structural properties, we have also studied the pressure induced transformation between two crystal structures of ZnS. ZnS adopts a rocksalt (NaCl) structure above a certain pressure [35]. In Figure 5.1, we have investigated the effect of pressure on the zinc-blende crystal structure of ZnS.

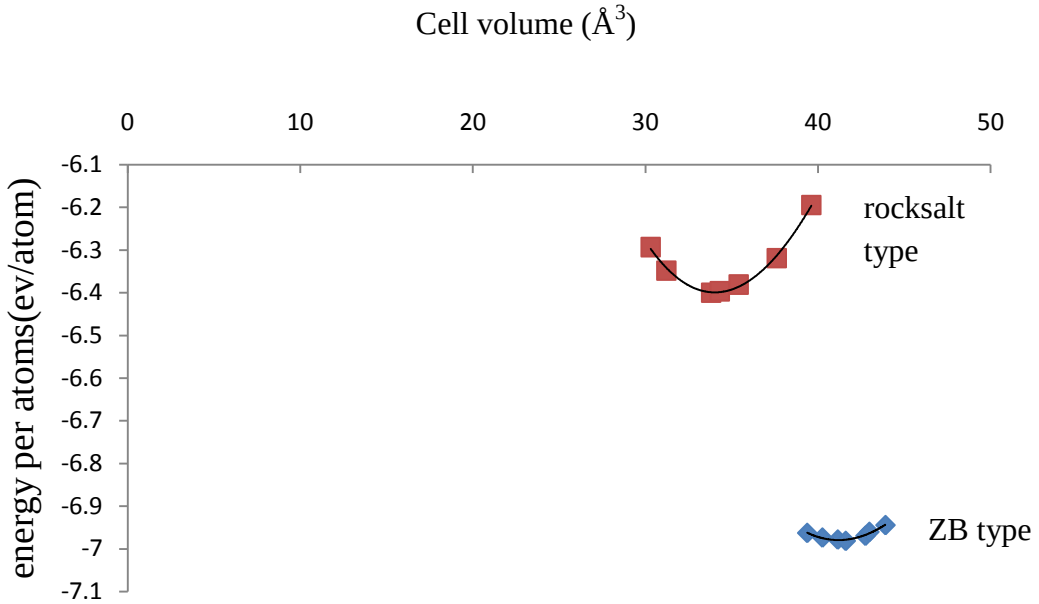

Figure 5.1: Variation of total energy with unit cell volume ($V = a^3$) for zinc-blende and rocksalt structures of ZnS. As pressure on the zinc-blende phase of ZnS increases (volume decreases), the rocksalt phase exists. Here, $E_{rocksalt} > E_{ZB}$ for all points shown.

The pressure induced structural phase transition in ZnS is studied by many authors with different computational methods. For example, M. Bilge et al.[36] revealed that the transition to the high pressure rock salt phase occurs at about 14.84 GPa.

5.1.1 Influence of Impurities on the ZnS Crystal Structure

The calculated lattice constant *a* of zinc-blende ZnS is 5.47 Å. Our result is in good agreement with the experimental value and other calculated results. From structural optimization calculations, we have found that incorporation of Mn and Cr impurities causes an expansion of ZnS crystal lattice. The calculated lattice constants of all compounds are listed in Table 5.2.

The expansion of the crystal lattice is due to the fact that each of the two incorporated impurities has a larger atomic radius, R_{Mn} = 0.179Å and R_{Cr} = 0.185Å, compared to that of Zn, which has an atomic radius of R_{Zn} = 0.153Å. Hence, the average bond length of Mn-S is longer than that of Zn-S. Similarly, the average bond length of Cr-S is larger than that of Zn-S.

Figures 5.2 (b) and (c) show that the shape of cubic structure is not changed after one Mn atom or one Cr atom has replaced one Zn atom at the lattice site. However, the lattice constant and local atomic positions are changed after introduction of Mn and Cr impurities into pure ZnS.

To study the effects of impurities on the electrical and optical properties of ZnS, we used 1x1x2 supercells for $ZnCrS_2$ and $ZnMnS_2$, while for Zn_3CrS_4 and Zn_3MnS_4, we used 2x2x1 supercells. The atomic valence electron configurations of Zn, S, Mn, and Cr are $3d^{10}4s^2$, $3s^23p^4$, $3d^54s^2$, and $3d^54s^1$, respectively. The $ZnMnS_2$ unit cell has 4 atoms with 29 electrons, the Zn_3MnS_4 unit cell has 8 atoms with 63 electrons, the $ZnCrS_2$ unit cell has 4 atoms with 28 electrons, and the Zn_3CrS_4 unit cell has 8 atoms with 62 electrons. In these unit cells, one Mn or one Cr atom has substituted one Zn atom. We have two types of S atoms in the unit cell: the one which directly bonded to the impurity atoms and the other which is not.

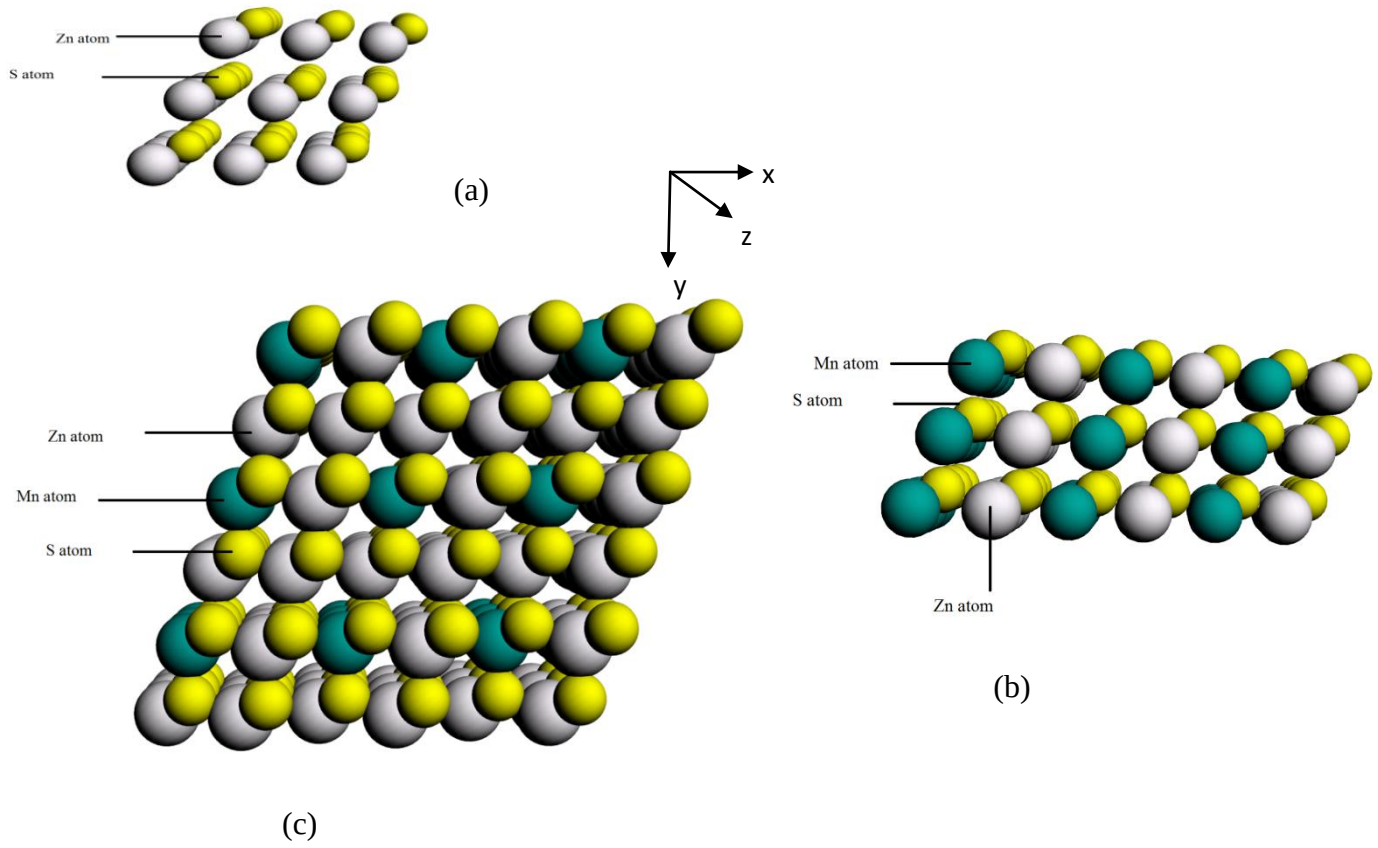

Figure 5.2: a) Crystalline ZnS; b) 1x1x2 Mn impurity substituted ZnS supercell $ZnMnS_2$; c) 2x2x1 Mn impurity substituted ZnS supercell Zn_3MnS_4.

Table 5.2: The optimized lattice constant of pure and doped ZnS, which will be used for further calculations in this project.

	Lattice constant (Å)		
Compounds	This work	Expt.	Other calculations
ZnS	5.47	5.41[a]	5.342[c]
MnS	5.68		
$ZnMnS_2$	5.56		
Zn_3MnS_4	5.50		
CrS	5.53		5.52[b]
$ZnCrS_2$	5.49		
Zn_3CrS_4	5.48		

[a]Reference 28 .

[b]Reference 37.

[c]Reference 38.

5.2 The Electronic Properties

In the first section of this project, the electronic structure of zinc-blende type ZnS, $Zn_{1-x}Mn_xS$ (x = 1, 0.5, 0.25), and $Zn_{1-x}Cr_xS$ (x = 1, 0.5, 0.25) is described in terms of electronic band structure and density of states (DOS). Partial density of states is important to know the different angular momentum component contributions. It provides information to identify the nature of orbitals, whether the states are s-like or p-like.

The Fermi energy (E_F), band gap, type of band gap, total and partial DOS, and the width of the valence and conduction bands are important information that can be extracted from electronic band structure calculations. It is very important to use a large number of k points to calculate the electronic band structure as the details of the electronic band structure come from integrals in k-space.

Here, the electronic states at the top of the valence bands and at the bottom of the conduction bands are investigated. Electrons deep down in the valence bands are basically frozen in their states and will not contribute to the electronic and optical properties of materials.

5.2.1 Electronic Properties of ZnS

In Figure 5.3, we present the calculated electronic band structure of zinc-blende ZnS at the predicted equilibrium lattice constant along the selected high symmetry *k* path within the first Brilloiun zone of its primitive cell, and in Table 5.3, we list the energy difference between the bottom of the conduction and the top of the valence band at high symmetry points in the Brillouin zone as determined from the periodic BAND program.

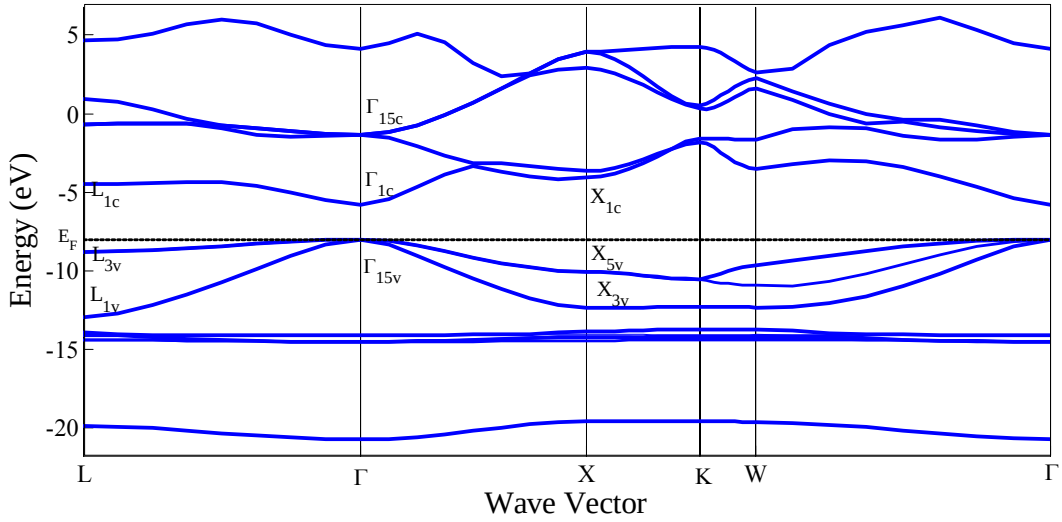

Figure 5.3: The calculated electronic band structure of ZnS along high symmetry points in the Brillouin zone.

The Fermi level is by definition, the energy where the probability is half for occupied state. For states with chemical potential (μ) = Fermi level (E_F), the Fermi distribution function f (μ) = 1/2 i.e. half of the states with μ = E_F are occupied.

The calculated electronic band structure shows zinc-blende ZnS is a direct band gap material with the top of the valence band and the bottom of the conduction band occurring at the zone center. We have found that the fundamental band gap or energy difference between the top of the valence band and the bottom of conduction band is 2.22 eV. At the point Γ the highest valence

band is doubly degenerate. The calculated band gap is underestimated in comparison with the experimental result, but the overall electronic band profiles are in fairly good agreement with the theoretical values [38].

Table 5.3: Band eigenvalues (in eV) at the high symmetry points within the Brillouin zone for the conduction band and the valence band of ZnS.

Location Brillouin zone	This work	Other Cal.	experiment
Γ_{15v} - Γ_{1c} (Band gap)	2.22	2.16[a]	3.80[b]
Γ_{15v} -X_{1c}	3.93	3.01[a]	4.10[a]
Γ_{15v} - L_{1c}	3.52	3.16[a]	4.40[a]
L_{3v} - L_{1c}	4.30	4.11[a]	
X_{5v} -X_{1c}	5.97	-	
Valence band width	12.59	13.41[a]	

[a]Reference 38.

[b]Reference 28.

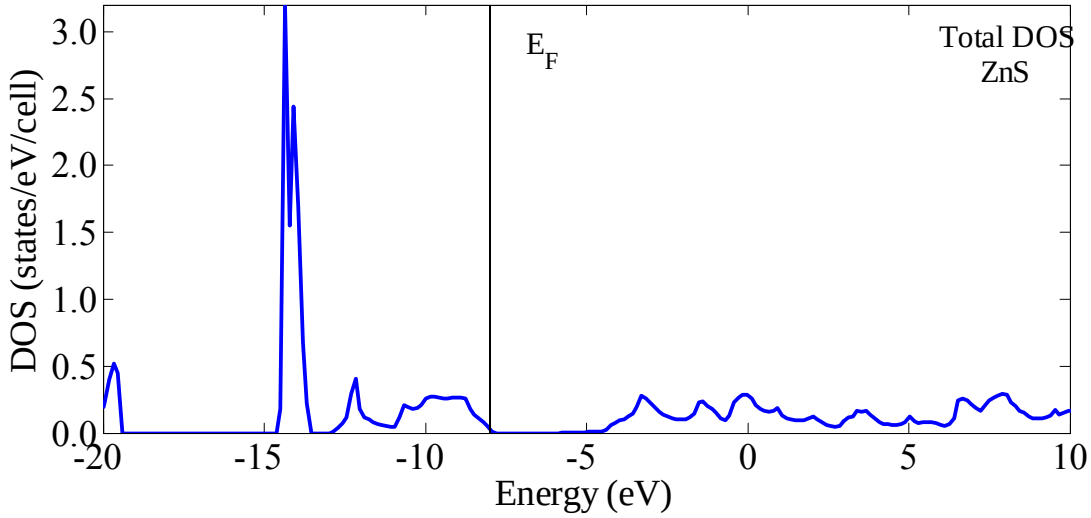

Figure 5.4: The calculated total density of states for ZnS when the top of the valence band was set at the Fermi level.

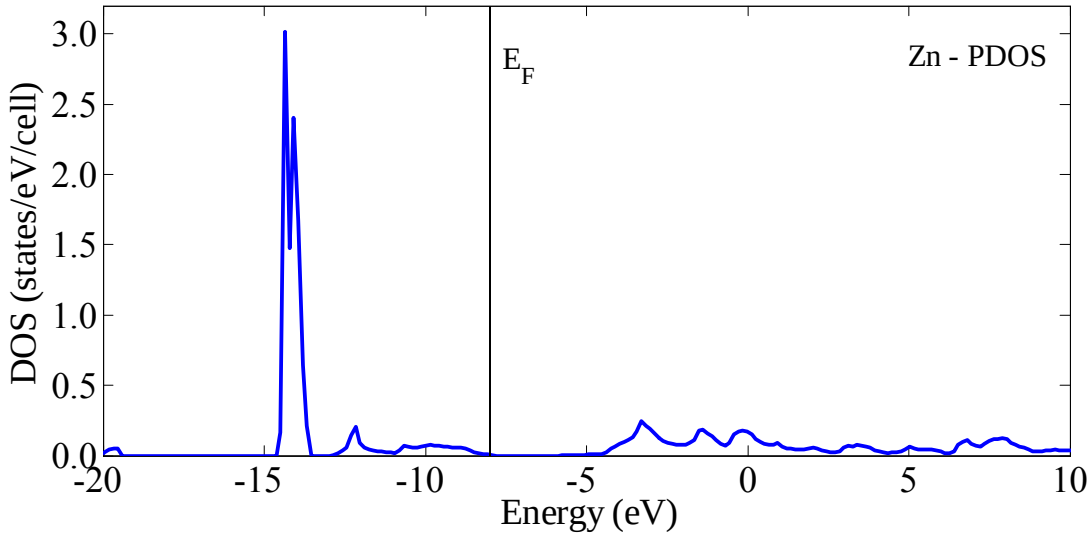

Figure 5.5: The calculated partial density of states of Zn atom with the valence electron configuration $3d^{10}\ 4s^{2}$.

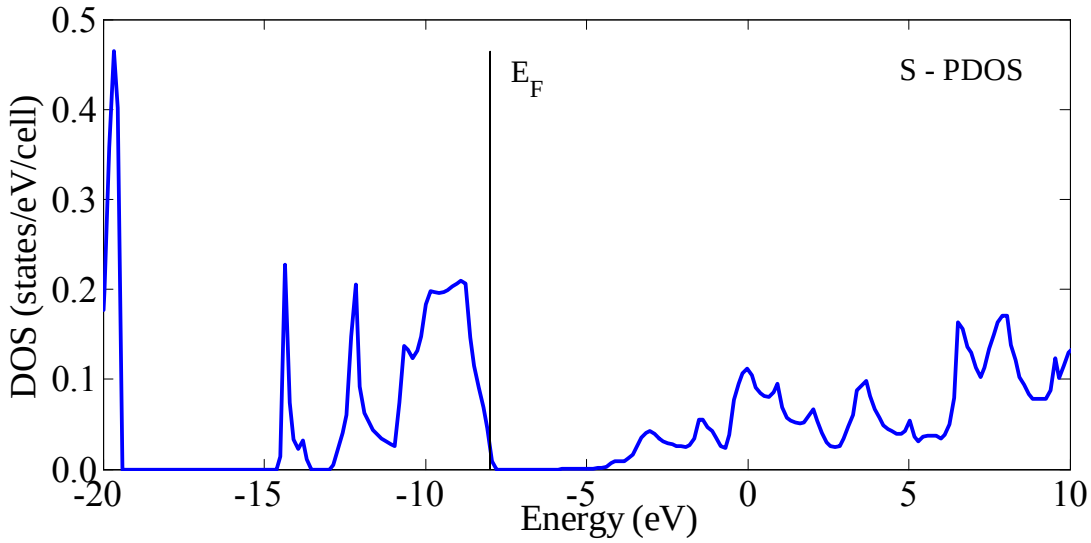

Figure 5.6: The calculated partial density of states of S atom with the valence electron configuration $3s^2\ 3p^4$.

The total DOS result in Figure 5.4 shows that the valence and conduction bands of ZnS are separated by band gap. For zinc-blende structure of ZnS, the valence band density of states may be divided into three regions. Using the valence band maximum as the Fermi level, the region around -13 eV is dominated by p-states from S atoms, with a small contribution of Zn s-states. The region around -14.5 eV to -13.5 eV is predominantly Zn d-states, with a small contribution from S p-states. This structure matches the flat bands in the electronic band structure of ZnS in Figure 5. 3. The total DOS furthest below the valence band, at around -20 eV, is mainly from the S s-states and it also matches with the lowest valence band in the calculated band structure of ZnS.

5.2.2 Electronic Properties of MnS

We performed spin-polarized ground state DFT calculations for zinc-blende MnS. For the treatment of electron exchange and correlation energies, we have used GGA-PW91.

The calculated electronic band structure E (k) for zinc-blende MnS at the equilibrium lattice constant a = 5.68 Å is given in Figure 5.7 along high symmetry points in the Brillouin zone of its primitive cell. From the electronic band structure calculation for majority-spin and minority-spin electrons, the results show that MnS is a narrow, direct gap magnetic semiconductor with the top of the valence band and the bottom of the conduction band occurs at the zone center. The calculated band gap for MnS is 0.084 eV at the Γ point. The Fermi level lies within the gap for spin-up and spin-down states.

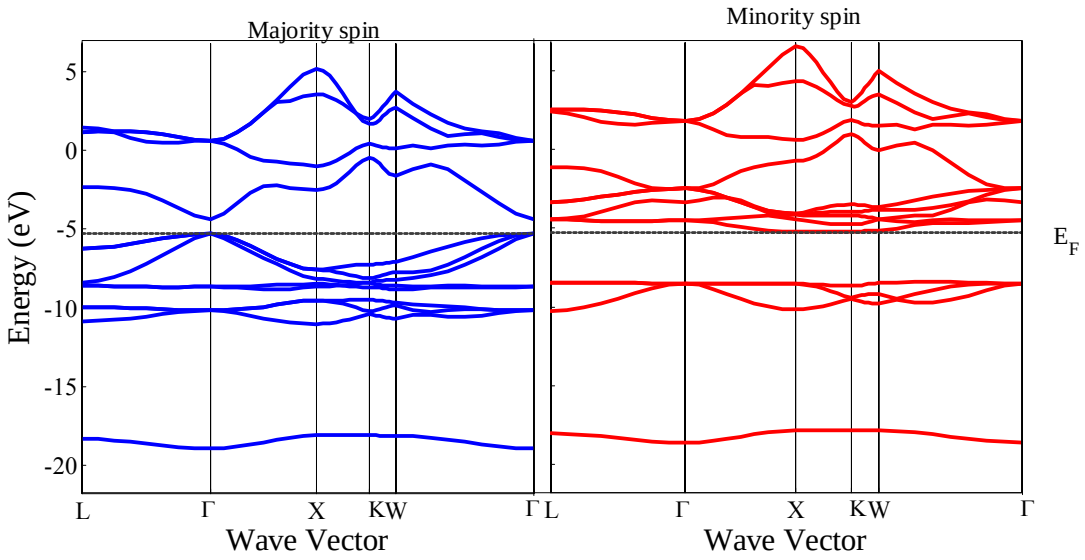

Figure 5.7: The calculated electronic band structure of MnS for the majority- spin electrons (spin-up states) and the minority- spin electrons (spin-down states).

In the case of minority-spin electrons the Mn atom 3d states plays an important role for the flatness of bands at the top of the valence and the bottom of the conduction bands. Unpaired spin orbitals are the origin of the magnetic properties of this compound. The calculated magnetic moments of zinc-blende MnS is $5\mu_B$ per MnS.

Figures 5.8 show that the calculated total density of states of MnS. From the partial density of states (PDOS) plots of MnS in Figure 5.9, we have found that d-states of the Mn atom at the top of the valence band is half-filled. As we know, materials in which the valence band is half-filled with electrons are called metals. Our results for the electronic band structure of zinc-blende MnS at the equilibrium lattice constant show small band gap value of 0.084 eV. This result contradicts the electronic band structure of metallic materials. However, we should be careful to reach conclusion on the band gap in DFT calculations. In metals, the Fermi surface separates the Brillouin zone into regions that are occupied and unoccupied by electrons. Calculating integrals in *k*-space is complicated in metals because of integration discontinuity [1]. Hence, to get well-converged results, metallic systems require a very much larger number of *k* points than semiconducting and insulating systems.

We have observed the convergence of the ground state energy up to KSPACE = 11, this also reduces the band gap energy to 0.052 eV. It might be necessary to increase the number of *k* points beyond KSPACE = 11 for ground state calculations of metallic systems. However, increasing the number of *k* points in the Brillouin zone (BZ) increases the computational time.

For the majority spin electrons, the feature in the density of states at the top valence bands originates mainly from the Mn d-states with a small contributions from the S p-states (see Figures 5.9 and 5.10).

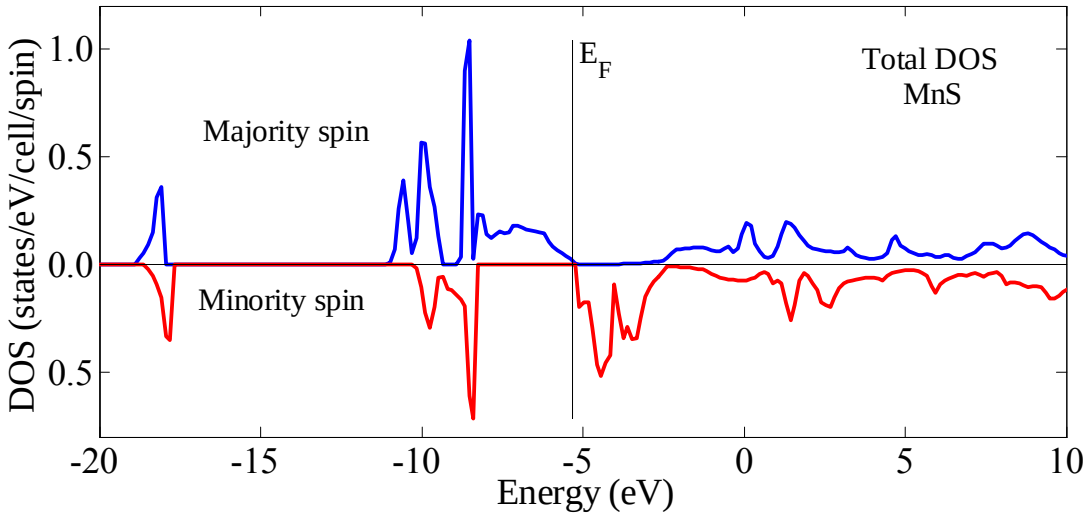

Figure 5.8: The calculated total density of states of MnS for the spin-up and spin-down electrons.

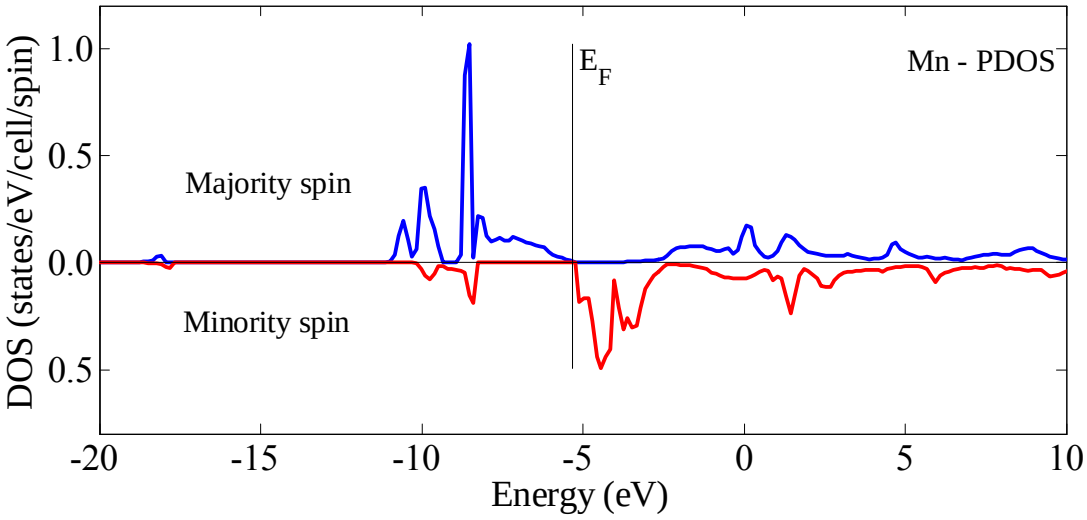

Figure 5.9: The calculated partial density of states of the Mn atom in MnS.

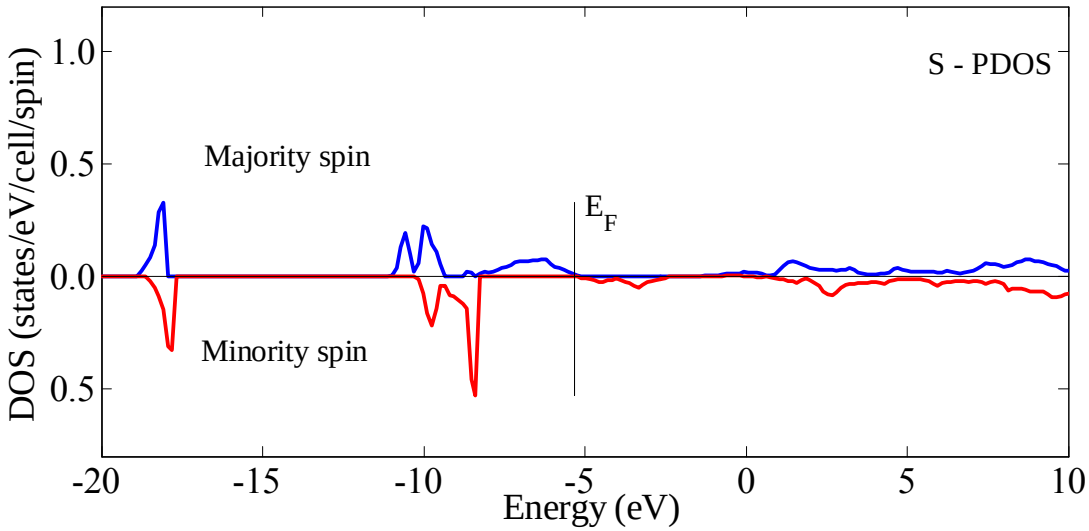

Figure 5.10: The calculated partial density of states of the S atom in MnS.

5.2.3 Magnetic Properties of CrS

For the zinc-blende type CrS we performed self-consistent spin-restricted and spin-polarized ground state DFT calculations. Figure 5.11 shows the calculated total energies as a function of lattice parameter for the non-magnetic (NM) and ferromagnetic (F) states of CrS. From these calculations, we have found that the ferromagnetic state is stable than the non-magnetic state of CrS. For the ferromagnetic state the calculated total energy as a function of lattice constant has a minimum at a = 5.53 Å.

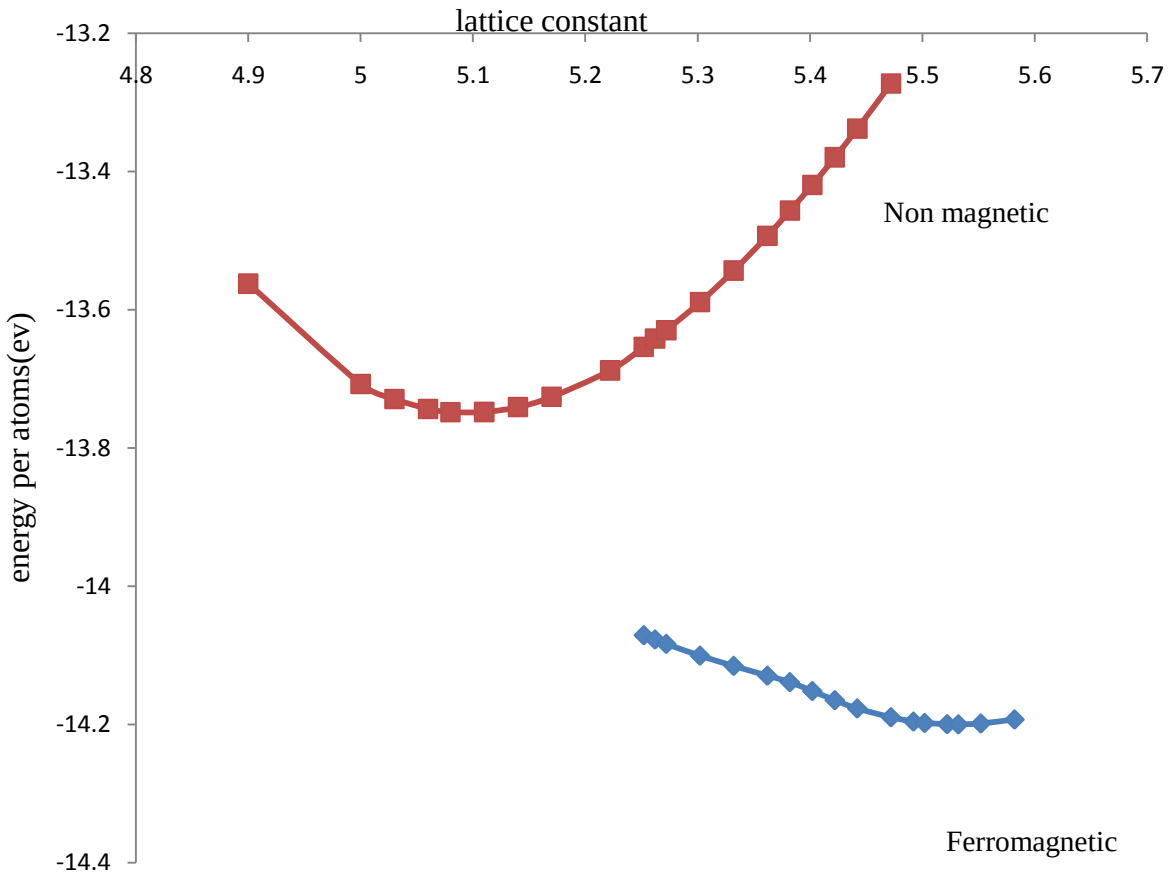

Figure 5.11: Total energy per unit cell as a function of lattice constant Å of CrS in the zinc-blende crystal structure.

5.2.4 Electronic Properties of CrS

Figure 5.12 shows the calculated electronic band structure of ferromagnetic CrS for the majority-spin and minority-spin electrons at the predicted equilibrium lattice constant. From features of the electronic band structure the majority-spin electron has metallic intersections, whereas the minority-spin electron has a semiconducting band gap across the Fermi level. From the electronic band calculations in Figure 5.12, we have found 0.32 eV a half metallic band gap of the minority-spin electrons at the bottom of the minority-spin electron conduction band. This is the minimum energy required to excite a spin-up electron from the top of the majority-spin

valence band to the minority-spin conduction band. The calculated electronic band structures for the majority and minority-spin electrons given in Figure 5.12 represent CrS.

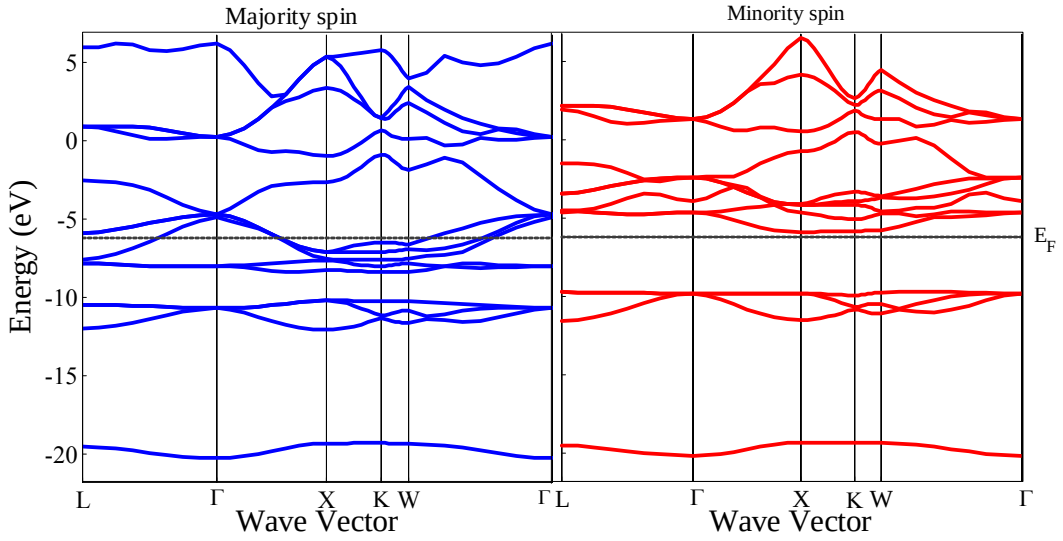

Figure 5.12: The electronic band structure of zinc-blende CrS for majority-spin electrons (spin-up) and minority-spin electrons (spin-down).

Figure 5.13 shows that the calculated total density of states of the ferromagnetic CrS is nonzero at the Fermi level for the majority-spin electrons. The majority-spin electrons are metallic, whereas for the minority-spin electrons, the Fermi level lies in the band gap. Therefore, the minority-spin electrons are semiconducting. Our results for the electronic band structure and total DOS show that CrS is half-metallic. Half-metallic materials are characterized by the coexistence of metallic and insulating behavior for the majority (spin-up) and minority (spin-down) electrons [6]. Other calculations reported by K.L.Yao et al. [37] based on plane-wave pseudopotential (PWPP) methods also reveal that zinc-blende CrS is half-metallic.

For majority-spin electrons, the feature in the DOS at Fermi level is the bonding states of hybrid S 3p and Cr 3d states which are recognized by the overlapping bands, whereas for the minority-spin electrons of CrS, the separation between the S 3p and Cr 3d states is large enough to create a band gap (see Figures 5.14 and 5.15). The anti bonding states have a higher energy than the bonding state. The total DOS at the Fermi level is mainly from the d states of the Cr atom. The magnetic moment M originates from spin polarization mainly from the Cr 3d states, as predicted

in the electronic structure calculations. The calculated magnetic moment of zinc-blende CrS is 4 μ_B per CrS.

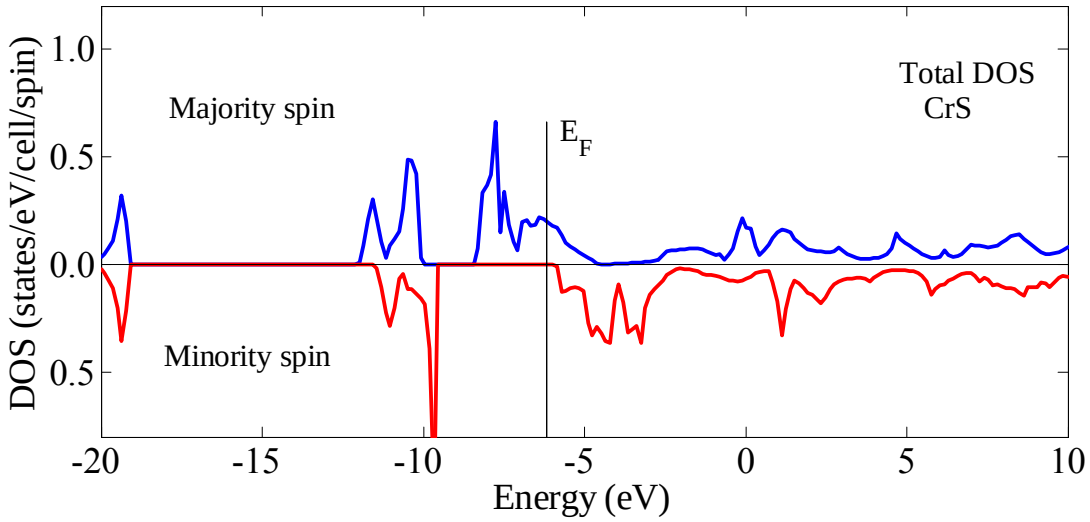

Figure 5.13: The calculated total density of states of CrS for the majority-spin (spin-up) and the minority-spin (spin-down) electrons.

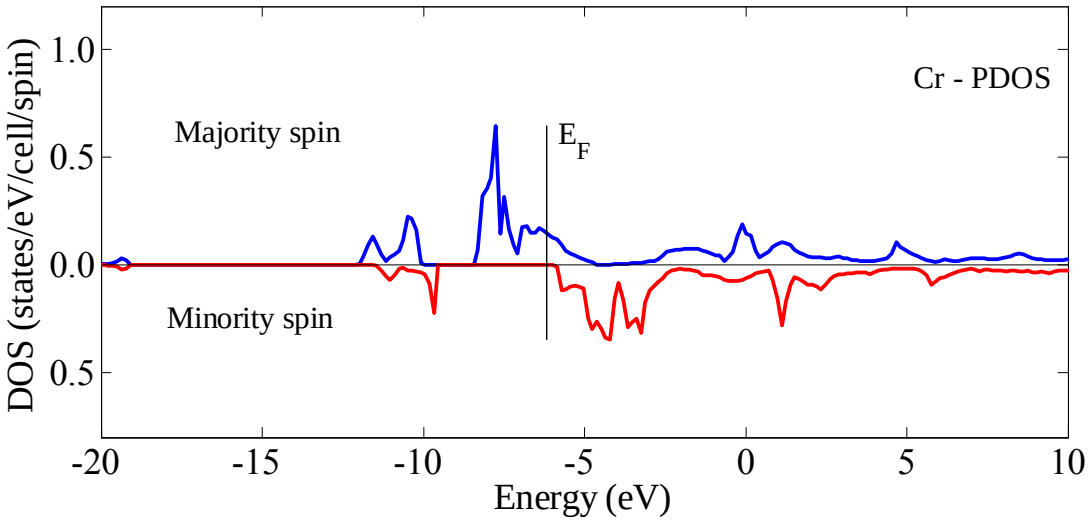

Figure 5.14: The calculated partial density of states of Cr in CrS.

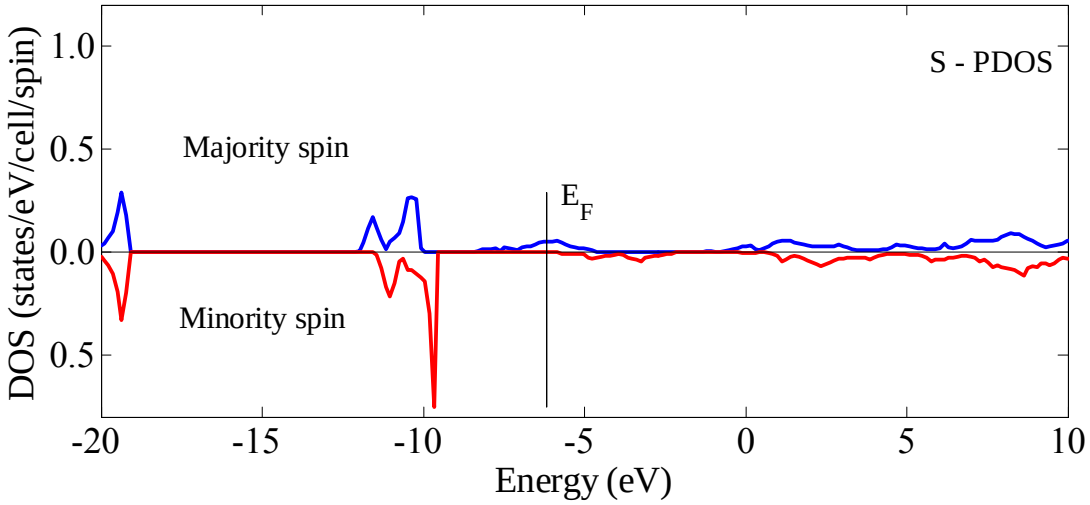

Figure 5.15: The calculated partial density of states of S in CrS.

5.3 Influence of Impurities on Electronic Structure

We have calculated the electronic band structure and the density of states of the magnetic semiconductors $Zn_{1-x}Mn_xS$ (x = 0.25, 0.5) and $Zn_{1-x}Cr_xS$ (x = 0.25, 0.5) in order to study the influence of Mn and Cr impurities on the electronic structure of ZnS. The Perdew-Wang (PW91) exchange and correlation functional within GGA is used for the treatment of the exchange and correlation effects.

5.3.1 Electronic Properties of $ZnMnS_2$

In Figure 5.16, we present the calculated spin-dependent electronic band structure for $ZnMnS_2$ at the predicted equilibrium lattice constant a = 5.56 Å along selected high symmetry lines in the Brillouin zone of its primitive cell. From the electronic band calculation results, we have found that the top of the valence band occurs at the zone center while the bottom of the conduction band does not occur at the center of the zone. The results show that bottom of the conduction band in $ZnMnS_2$ is found at point **k** = (0.028, 0.436, 0.364). This is a point on the line joining the center of the zone (Γ point) and the midpoint of a hexagonal face (L point) or along the line Λ. Hence, $ZnMnS_2$ is an indirect, narrow band gap semiconductor.

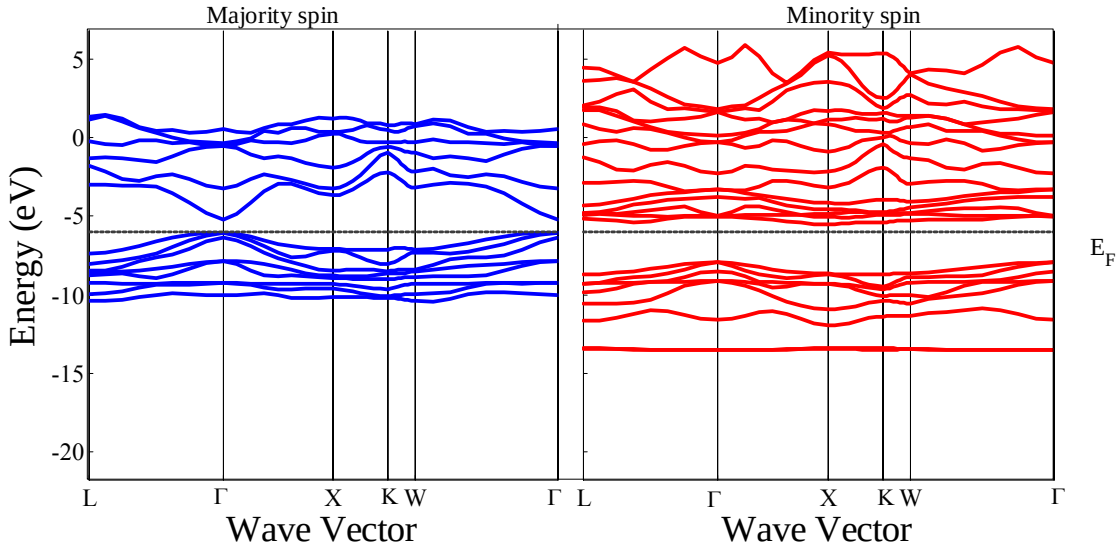

Figure 5.16: The calculated electronic band structure of $ZnMnS_2$ for the majority and minority -spin electrons at the predicted equilibrium lattice constant**.**

Mn impurity substitution for Zn atoms introduces bulk defect states within the band gap. The energy level change around the Fermi level makes the band gap of zinc-blende $ZnMnS_2$ smaller.

Figure 5.17 shows that the total density of states of ZnS shifts to higher energy by about 1.95 eV from the Fermi level due to the introduction of the Mn impurity. Therefore, the substitution of Mn impurity into pure ZnS, increases the lattice constant, and changes the position of the valence and the conduction bands. The Fermi level is also changed. The energy level change around the Fermi level makes the band gap of $ZnMnS_2$ decrease to 0.44eV. It can be seen clearly from the PDOS in Figures 5.19 and 5.20, the total density of states at the top of the valence bands is mainly from the Mn 3d states with a small contributions from the S 3p states. Figure 5.18 shows that the conduction band is partially from s- and p-states of Zn atoms.

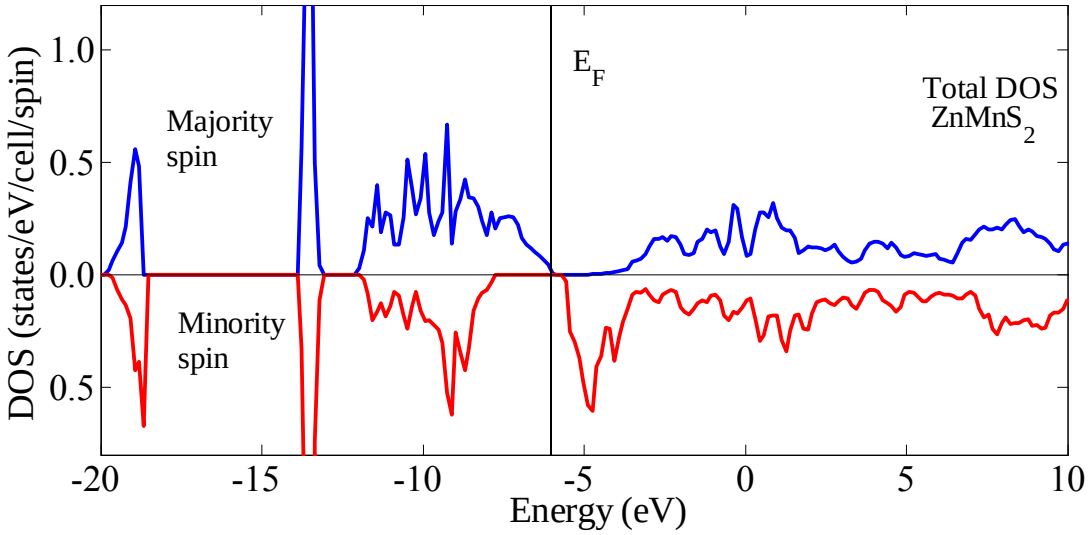

Figure 5.17: The calculated total density of states of $ZnMnS_2$.

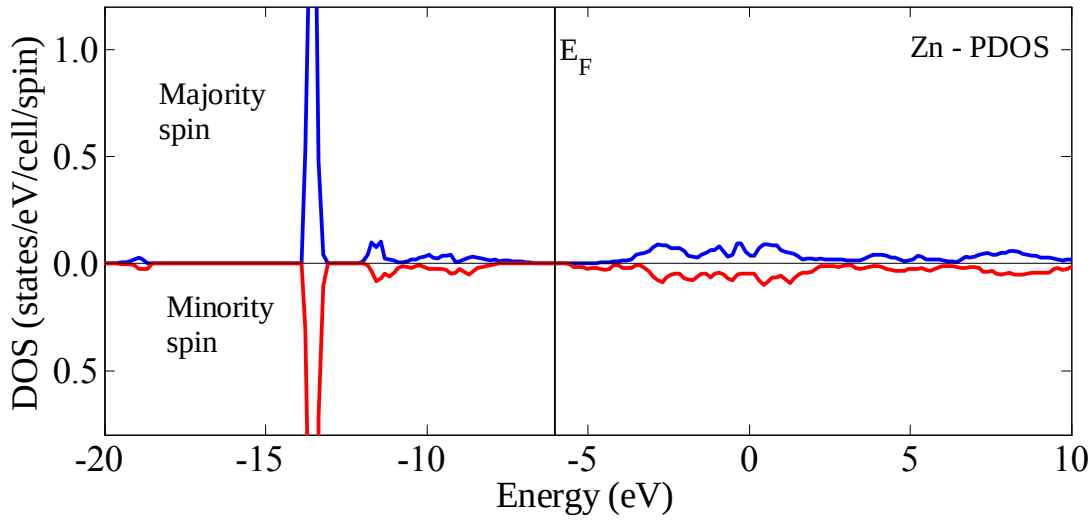

Figure 5.18: The calculated partial density of states of Zn atom in $ZnMnS_2$.

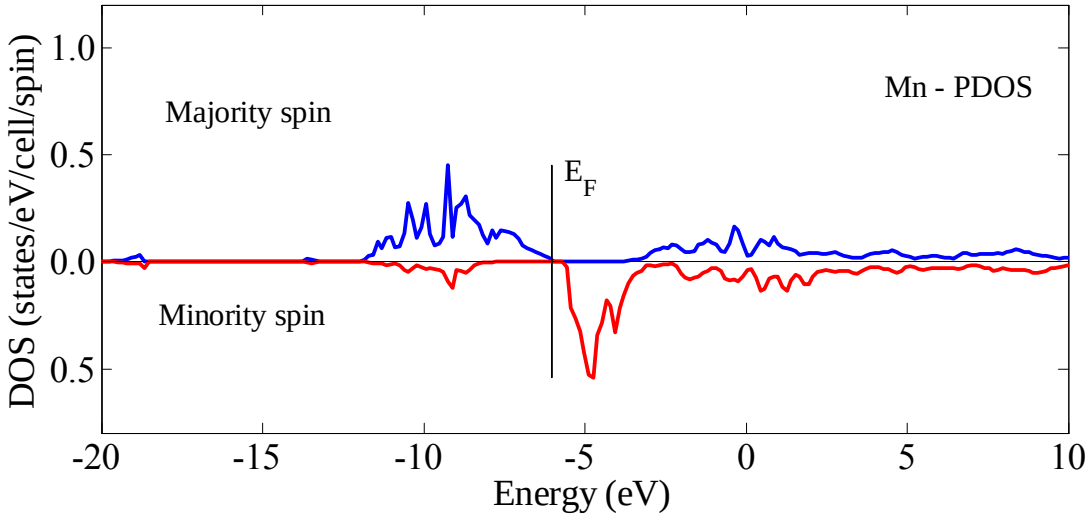

Figure 5.19: The calculated partial density of states of Mn atom in $ZnMnS_2$.

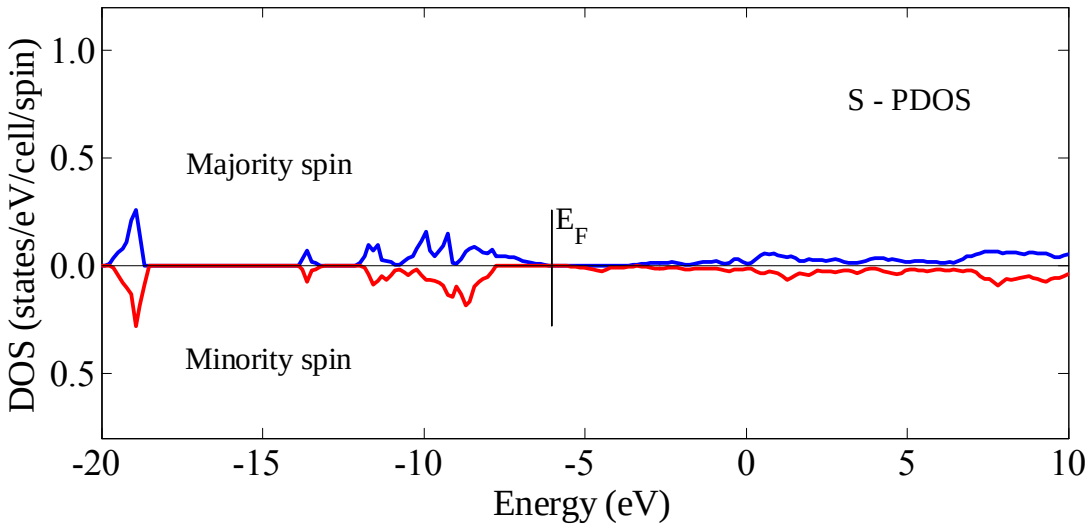

Figure 5.20: The calculated partial density of S atom in $ZnMnS_2$.

5.3.2 Electronic Properties of Zn_3MnS_4

Figure 5.21 shows the calculated electronic band structure of Zn_3MnS_4 for the majority and minority-spin electrons at the predicted equilibrium lattice constan a = 5.50 Å. From the electronic band calculations of Zn_3MnS_4, we have found that the top of the valence band and the bottom of the conduction band occur at the zone center. Hence, zinc-blende Zn_3MnS_4 is a direct, small band gap semiconductor. Figure 5.22 shows that the total density of states of ZnS

shifts to higher energy by about 1.35 eV due to the introduction of 25% Mn impurities. This result shows that the conductivity of $ZnMnS_2$ is higher than that of Zn_3MnS_4. Our results for the electronic band structure show that introducing a high Mn impurity concentration into pure ZnS forms band-like states near the conduction band edge, and the Fermi level lies within this band.

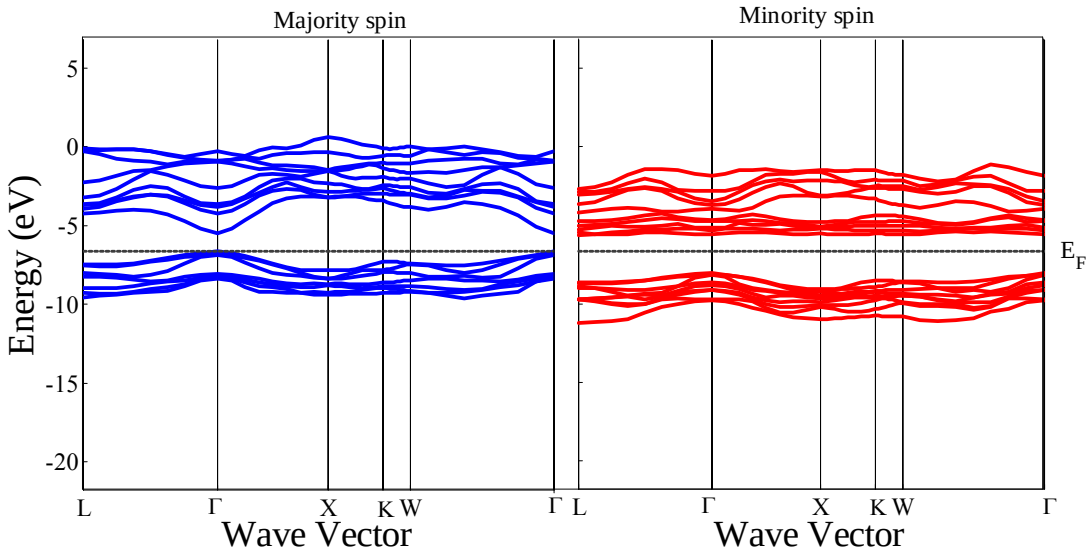

Figure 5.21: The calculated electronic band structure of Zn_3MnS_4 for the majority- spin electrons and the minority- spin electrons.

From the PDOS plot of Zn_3MnS_4 in Figures 5.23 and 5.25 the value of the total DOS in the valence band near the Fermi level is mainly from the Mn d-states with a small contribution from the S 3p states. We can also see that the Mn d-states for the majority-spin electrons lie deep in the valence band, whereas for minority-spin electrons, the Mn d-states are located in the shallow conduction band. Figure 5.24 shows that the conduction band is partially from s- and p-states of Zn atoms.

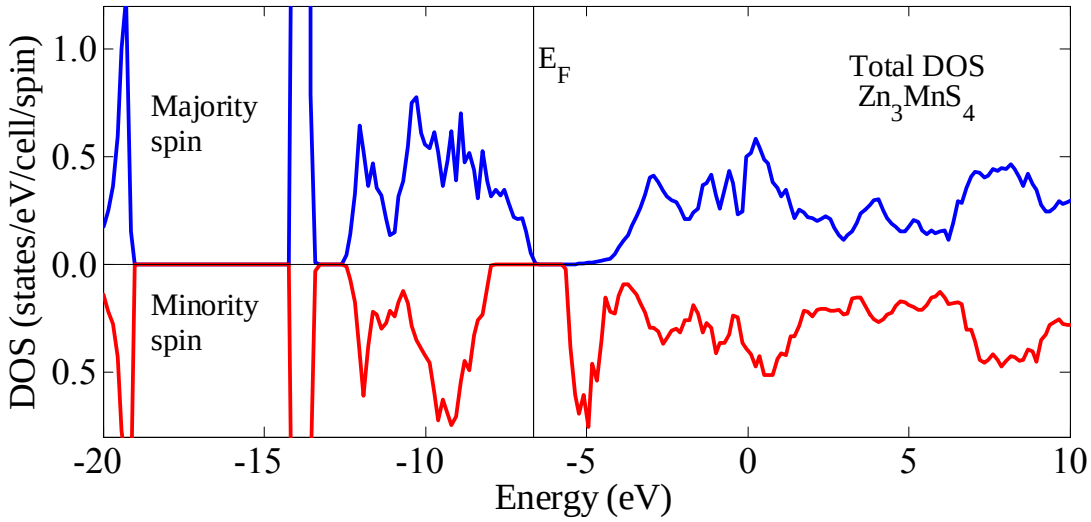

Figure 5.22: The calculated total density of states of Zn_3MnS_4.

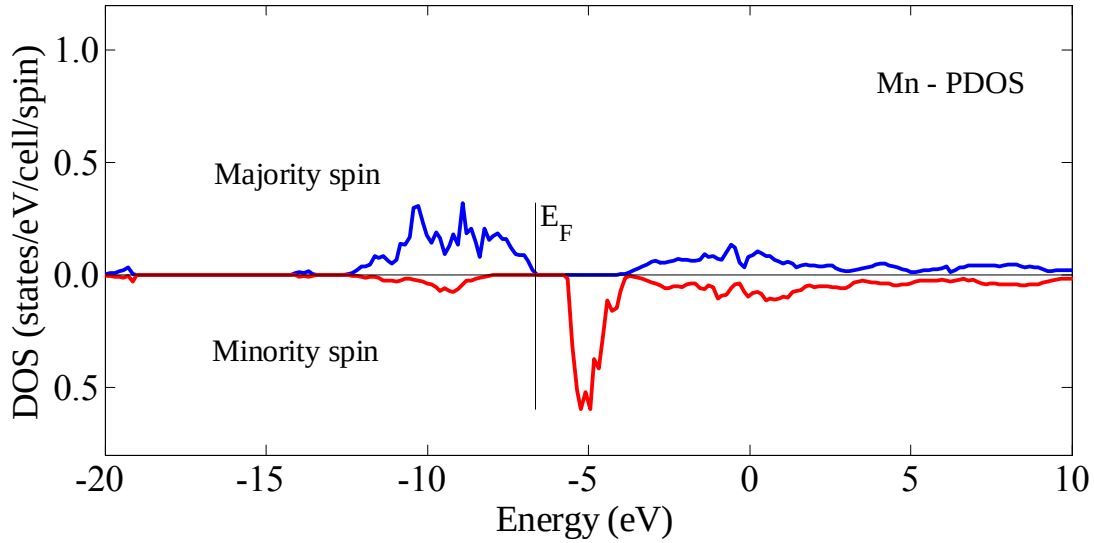

Figure 5.23: The calculated partial density of states of Mn atom in Zn_3MnS_4.

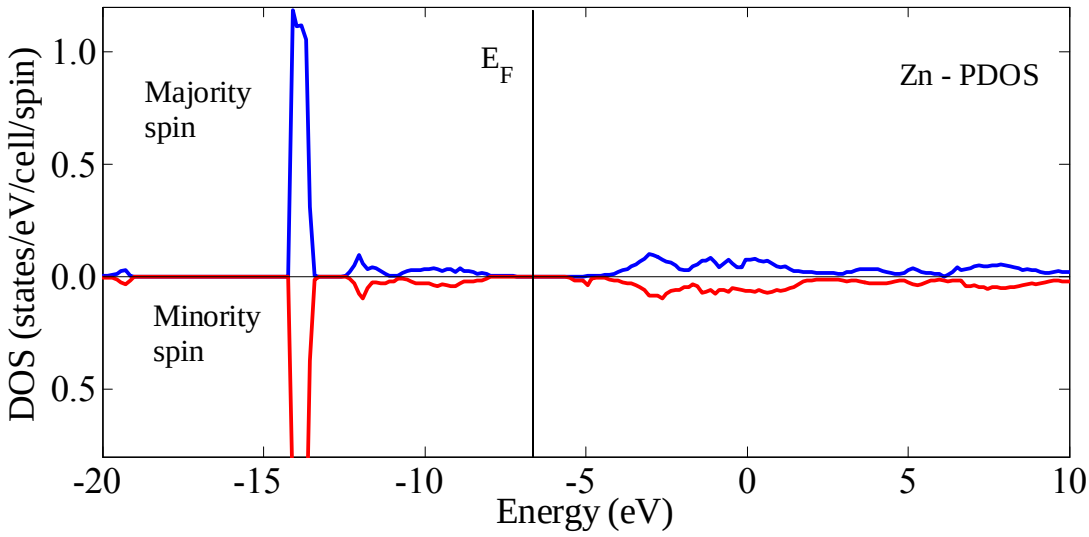

Figure 5.24: The calculated partial density of states of Zn atom in Zn_3MnS_4.

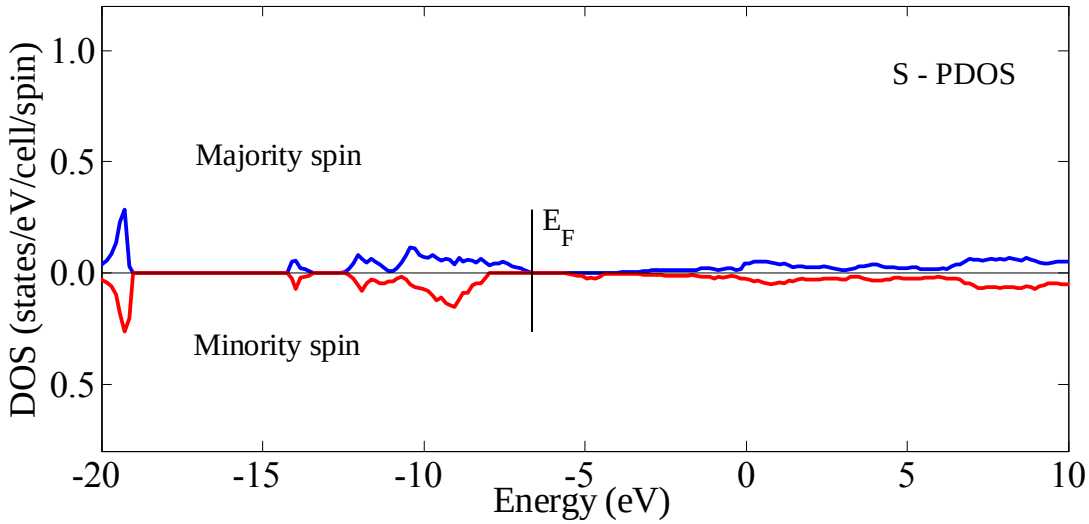

Figure 5.25: The calculated partial density of states of S atom in Zn_3MnS_4.

It can be seen clearly either from the calculated electronic band structure or from the total density of states in Figures 5.21 and 5.22 respectively, the Mn impurities mainly affect the shallow conduction bands and the deep valence bands of ZnS.

Figure 5.26 compares the total DOS of pure ZnS and Mn impurity substituted ZnS. As the lattice constant increases in the order $ZnMnS_2$ > Zn_3MnS_4 > ZnS, the width of the valence band

increases accordingly. The narrow band gap of $ZnMnS_2$ and Zn_3MnS_4 is due to the introduction of impurity states in the valence band near the Fermi level.

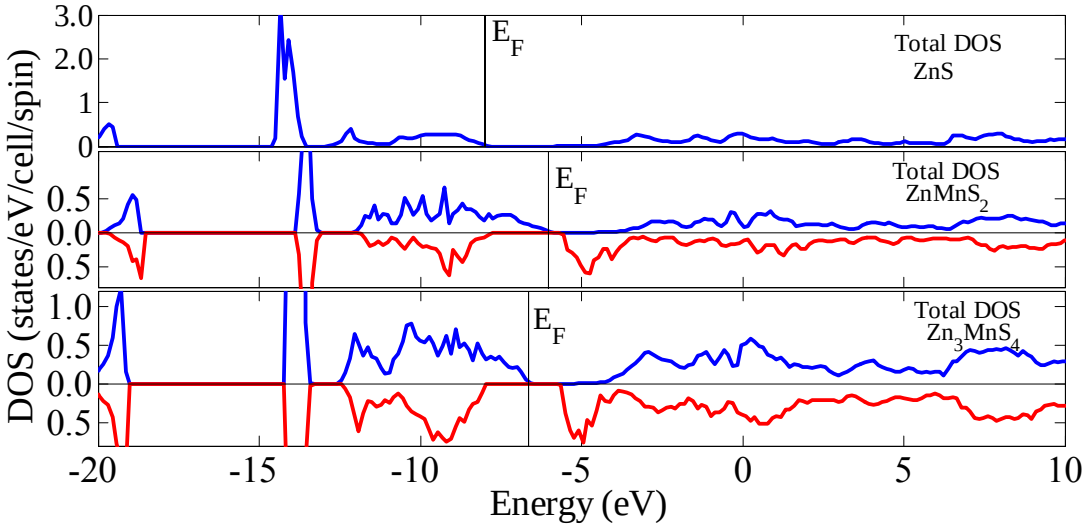

Figure 5.26: The calculated total density of states of ZnS, $ZnMnS_2$, and Zn_3MnS_4.

5.3.3 Electronic properties of $ZnCrS_2$

Figure 5.27 shows the calculated spin dependent electronic band structure of $ZnCrS_2$ at the predicted equilibrium lattice constant a = 5.68 Å. The result shows a half-metallic behavior in $ZnCrS_2$. We have also found that the half-metallic band gap is 0.80 eV.

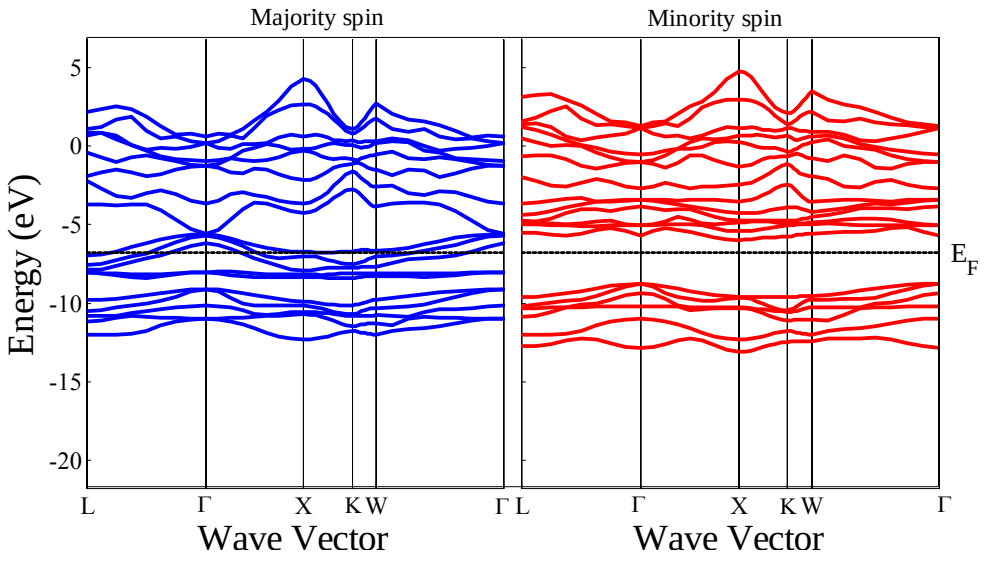

Figure 5.27: The calculated electronic band structure of $ZnCrS_2$ for the majority (spin-up) and for the minority (spin-down) electrons.

Figure 5.28 shows the calculated total density of states of $ZnCrS_2$. For the majority spin electrons the features in the density of states at the Fermi level is mainly from Cr 3d states with a small contribution from the S 3p states (see Figures 5.29 and 5.31). Figure 5.30 shows that the conduction band is partially from s- and p-states of Zn atoms. We have found that the Cr impurity mainly affects the shallow and deep valence bands.

Our results for the total density of states show that Cr impurity substitution into pure ZnS introduces impurity states within the band gap, changes the position of the conduction and valence bands, and increases the lattice constant of the cell. The Fermi level is also changed. Figure 5.28 shows that the total density of states of ZnS shifts to higher energy by 1.2 eV from the Fermi level due to the introduction of 50 % Cr impurities.

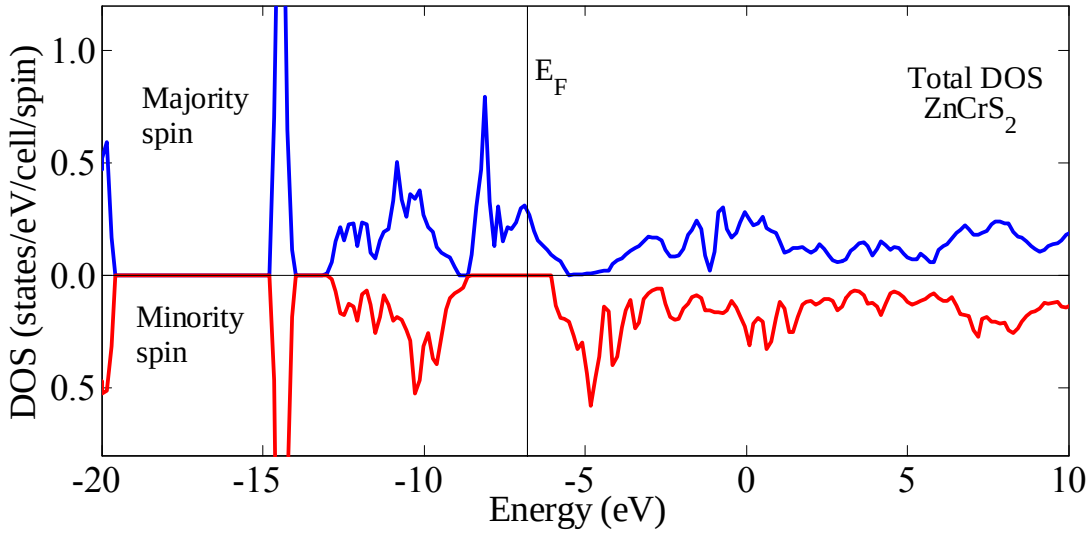

Figure 5.28: The calculated total density of states of $ZnCrS_2$.

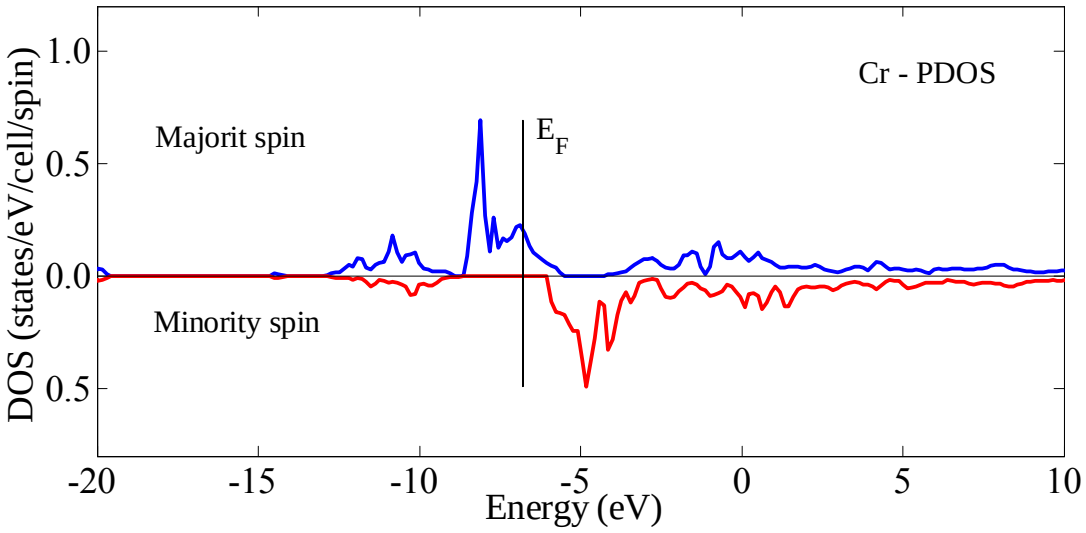

Figure 5.29: The calculated partial density of states of Cr atom in $ZnCrS_2$.

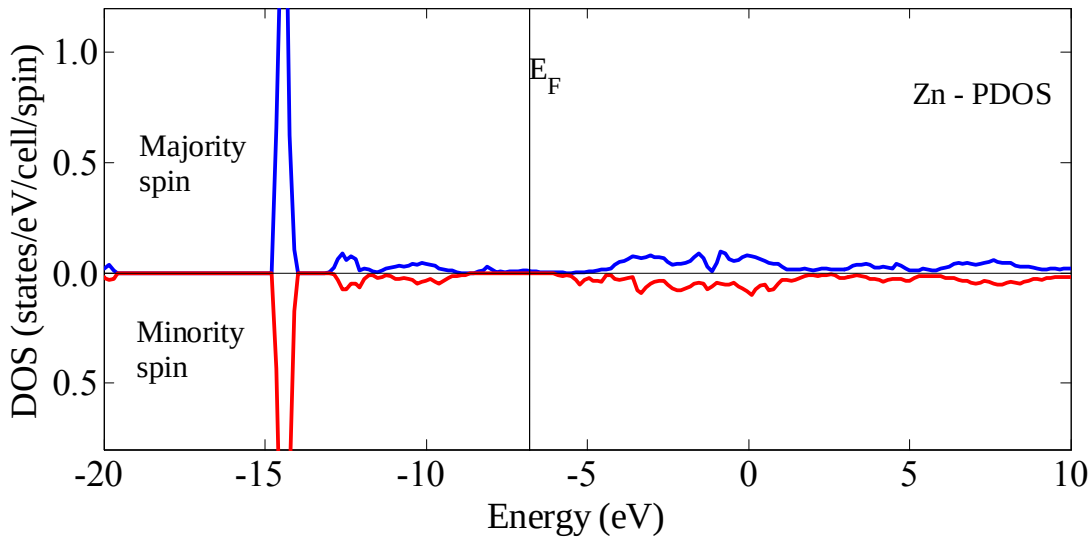

Figure 5.30: The calculated partial density of states of Zn atom in $ZnCrS_2$.

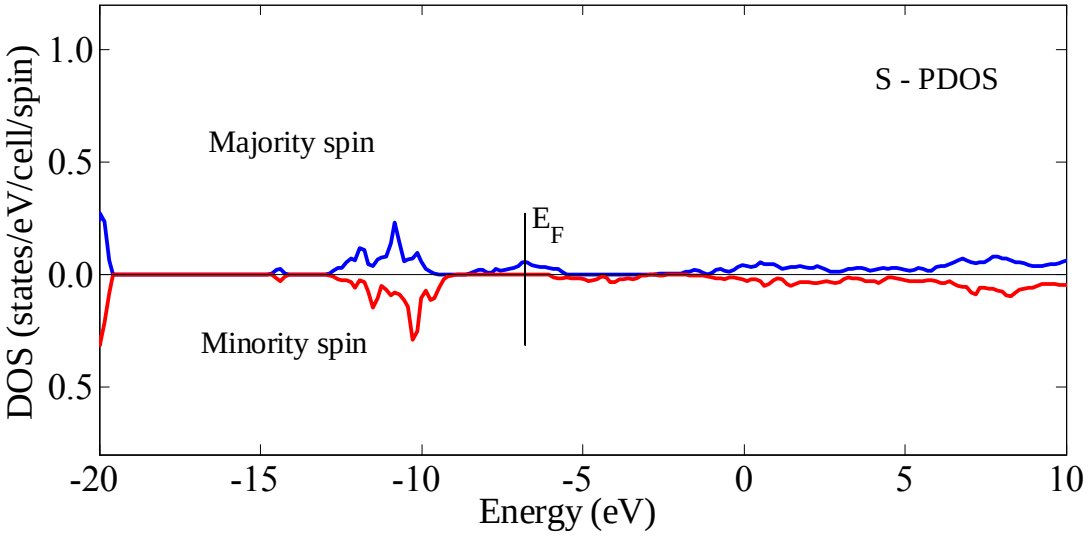

Figure 5.31: The calculated partial density of states of S atom in $ZnCrS_2$.

5.3.4 Electronic Properties of Zn_3CrS_4

Figure 5.32 shows the calculated spin-dependent electronic band structure of Zn_3CrS_4 for the majority and minority spin electrons at the predicted equilibrium lattice constant a = 5.48 Å along selected high symmetry k path within the Brillouin zone of its primitive cell.

From the electronic band structure calculation results, we have found a half-metallic behavior in Zn_3CrS_4. We have also found that the half-metallic band gap is 0.99 eV at the zone center Γ.

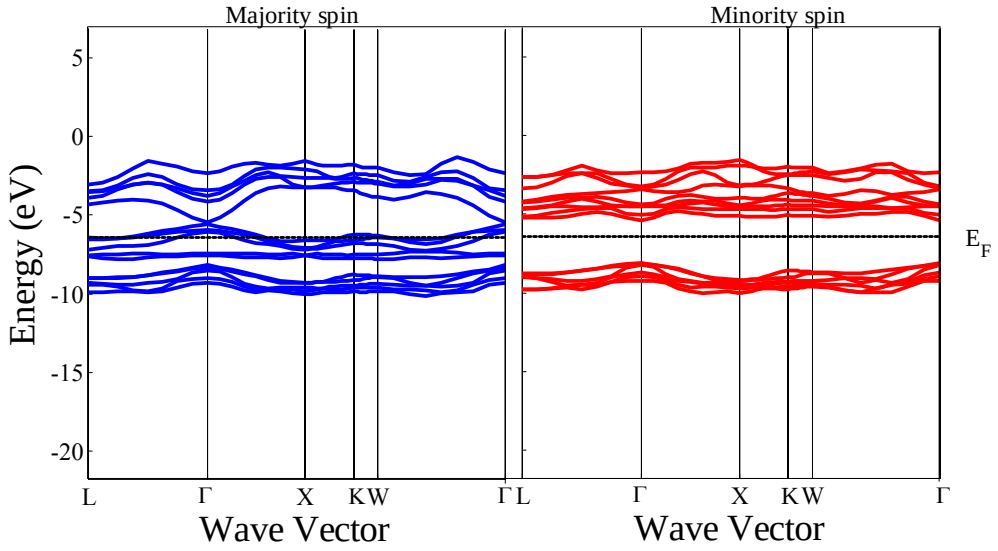

Figure 5.32: The calculated electronic band structure of Zn_3CrS_4 for the majority (spin-up) and for the minority (spin-down) electrons.

Figure 5.33 shows the calculated total density of states of Zn_3CrS_4. Our result shows that the total density of states at the Fermi level is mainly from Cr d states with a very small contribution from S p states (see Figures 5.34 and 5.36). Figure 5.35 shows that the conduction band is partially from s- and p-states of Zn atom. The energy level change around the Fermi level makes the band gap of this material decrease to 0.99 eV.

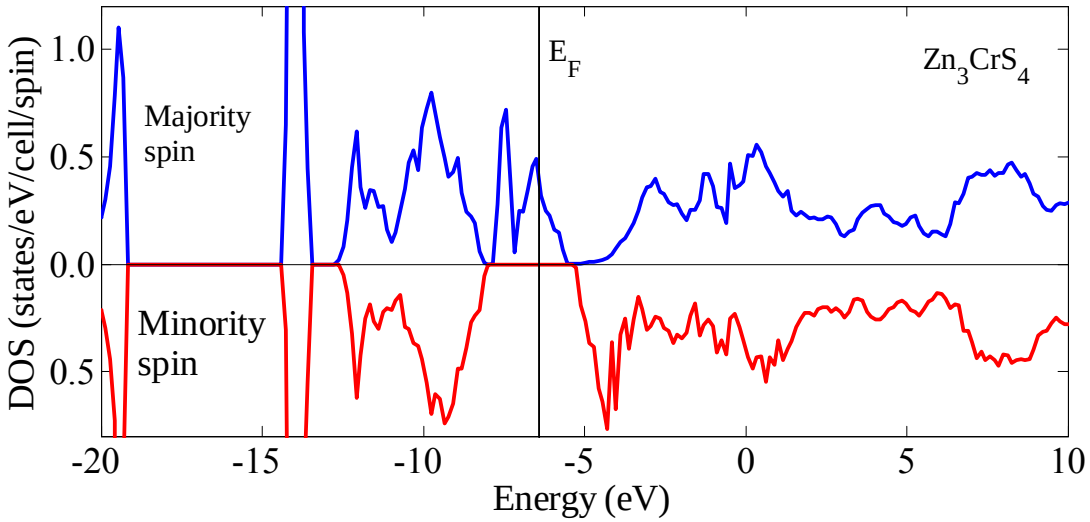

Figure5.33: The calculated total density of states of Zn_3CrS_4.

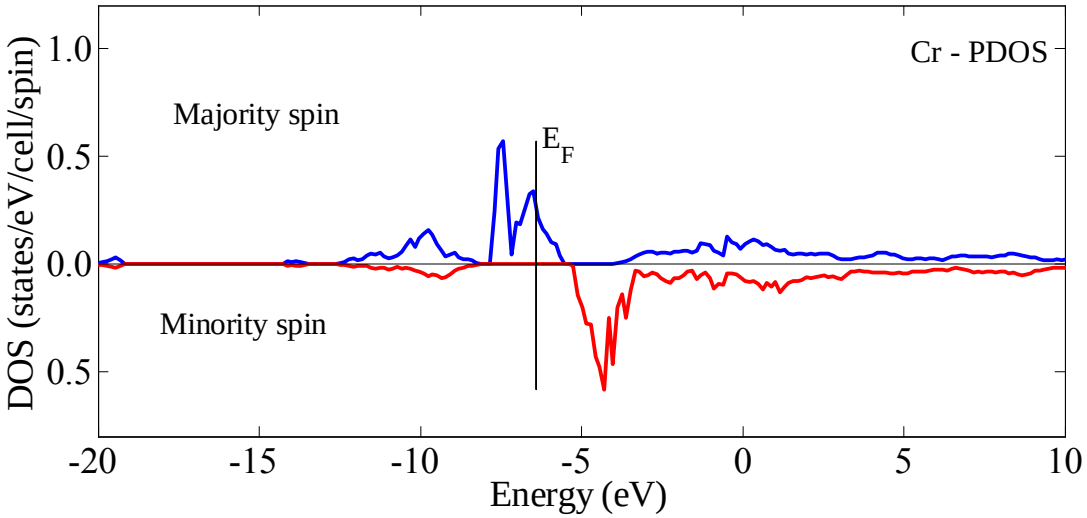

Figure 5.34: The calculated partial density of states of Cr atom in Zn_3CrS_4.

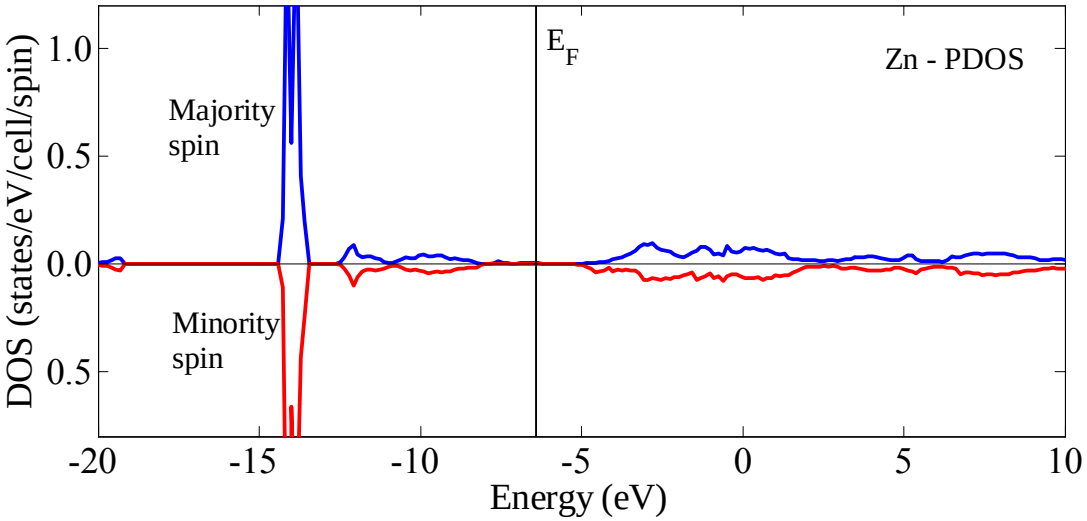

Figure 5.35: The calculated partial density of states of Zn atom in Zn_3CrS_4.

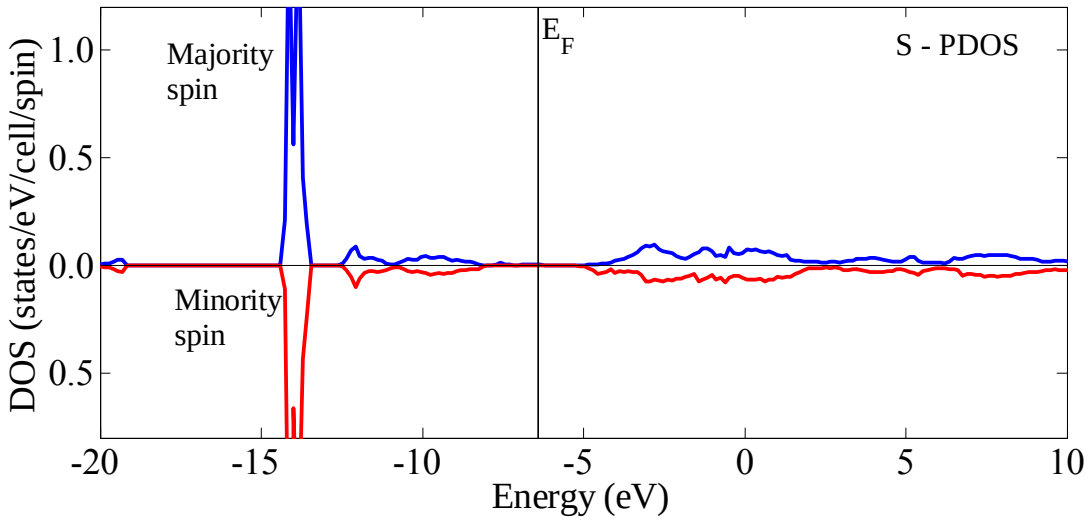

Figure 5.36: The calculated partial density of states of S atom in Zn_3CrS_4.

It can be seen clearly in Figure 5.37 that the total density of states of ZnS shifts to higher energy by 1.2 eV from the Fermi level due to the introduction of 50 % Cr impurities. At the same time, our result shows that the total density of states of ZnS shifts to higher energy by 1.59 eV from the Fermi level due to the introduction of 25% Cr impurities.

Figure 5.37 show that Cr impurities mainly affect the shallow and deep valence bands. The impurity level located close to the edge of the valence band is called a shallow level, and the one further from the edge is called a deep level.

The overall features of the density of states for $ZnCrS_2$ and Zn_3CrS_4 are quite similar except the position of the Fermi level.

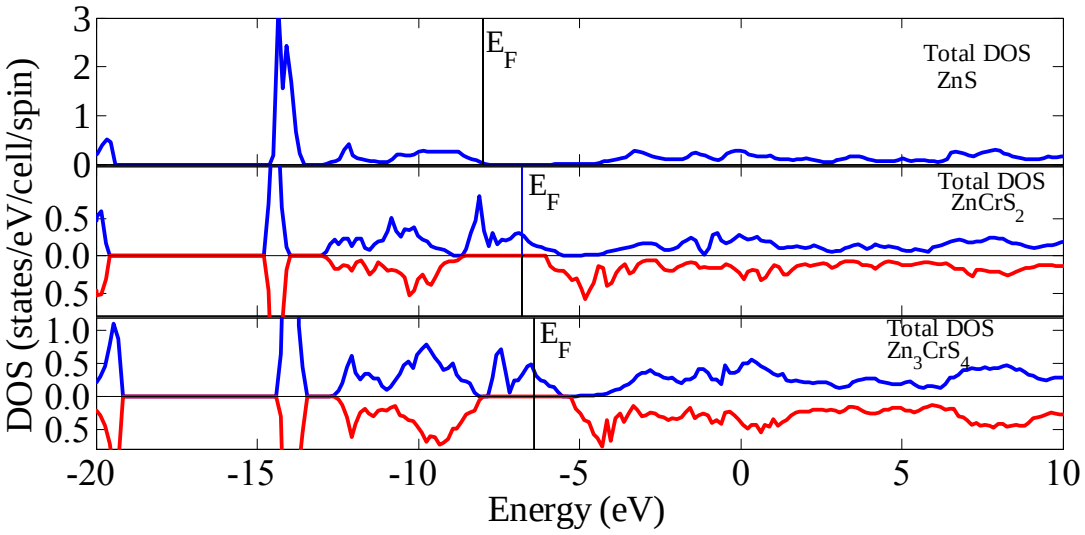

Figure 5.37: The calculated total density of states of ZnS, $ZnCrS_2$, and Zn_3CrS_4.

Table 5.4: The calculated band gaps of ZnS, $Zn_{1-x}MnS_x$ (x = 1, 0.5, 0.25) and $Zn_{1-x}CrS_x$ (x = 1, 0.5, 0.25).

Compounds	Band gap (eV)	other Cal.
ZnS	2.22	
MnS	0.08	
CrS	0.32	0.39[a]
$ZnCrS_2$	0.80	
Zn_3CrS_4	0.99	
$ZnMnS_2$	0.44	
Zn_3MnS_4	0.97	

[a]Reference 37.

5.4 Optical properties

We present the time dependent density functional theory calculation results for the real and imaginary components of the frequency dependent dielectric function of zinc-blende pure ZnS. The dielectric functions are also calculated to study influence of Mn and Cr impurities on the optical properties of ZnS for 1x1x2 supercells. The calculation was performed using GGA-PW91 for the treatment of electron exchange and correlation energies. Sampling of the Brillouin zone was done with KSPACE = 5.

The analysis of the overall spectrum provide important information about electronic band structure at *k* points in the Brillouin zone, in particular at points of high symmetry near the valence and conduction band edges. The *x*, *y*, and *z* axes are indistinguishable in cubic crystals. Hence, zinc-blende ZnS, $ZnMnS_2$, and $ZnCrS_2$ have isotropic optical properties.

5.4.1 Optical Properties of Zinc-blende ZnS

Figure 5.38 shows the real and imaginary components of the frequency dependent dielectric function of ZnS. Our results are in a good agreement with other theoretical results and experimental values.

The calculated real part of the dielectric function $\varepsilon_1(\omega)$ for the low frequency electric fields is given in Table 5.5. In this project, the subscript on ε_∞ represents dielectric response to the low frequency electric fields.

Table 5.5: The calculated static dielectric constant ε_∞ of ZnS.

Compound	This work	Expt.	Other theory
ZnS	5.62	5.2 (Ref. 21)	5.71 (Ref. 21)

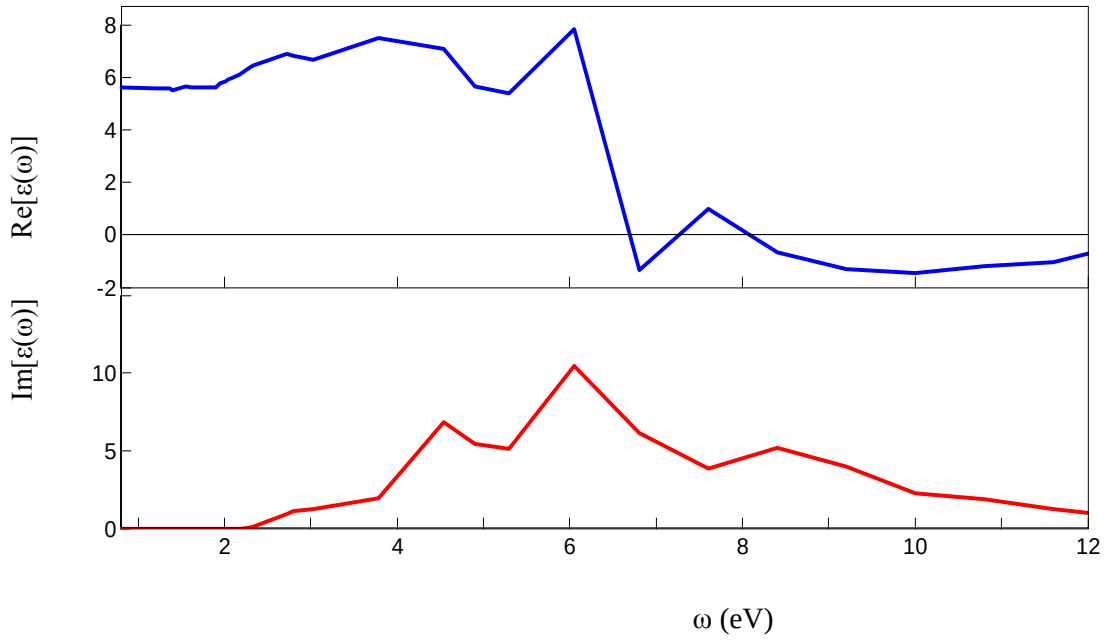

Figure 5.38: The calculated real and imaginary component of the dielectric function ε(ω) of pure ZnS.

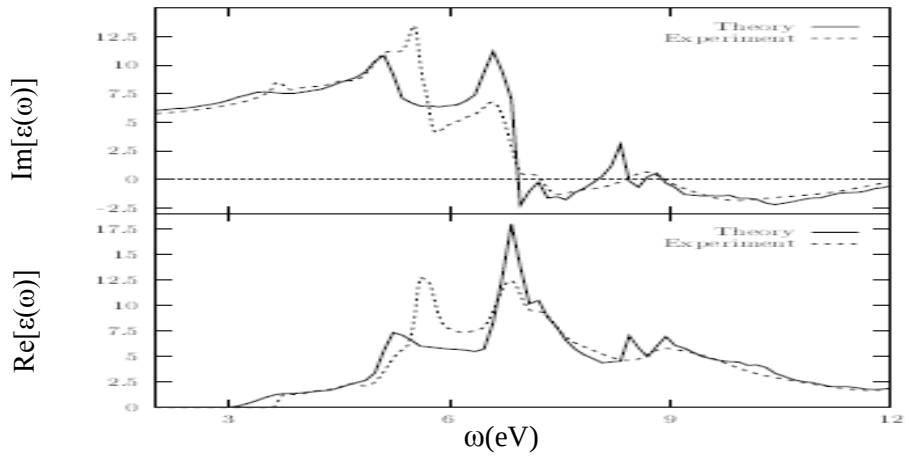

Figure 5.39: Theoretical and experimental results of real and imaginary components of dielectric function ε(ω) of ZnS (Figure adopted from Ref. 21).

The imaginary part of dielectric function is related to the absorption spectrum. Here, we calculate the frequency dependent dielectric function in the spectral range 0 - 14 eV. It can be seen clearly in the features of the optical absorption spectra in Figure 5.38 that there is no absorption at excitation energies less than band gap. For pure ZnS, the absorption spectrum from the fundamental absorption edge at about 2.22 eV to 14 eV is interpreted by direct interband transitions from the top of the valence bands $L_{1v} - \Gamma_{15v} - X_{5v}$ to the lowest conduction bands $L_{1c} - \Gamma_{1c} - X_{1c}$.

Figure 5.38 shows a shoulder and peaks in the absorption spectrum at critical points. The sharp peak at about 6.05 eV in Figure 5.38 corresponds to a direct interband transition at the point $X_{5v} - X_{1c}$. Our result indicates that the strong direct absorption at the sharp peak in the spectral region around 6.05 eV is due to a high density of states at X point (see the calculated band structure and total DOS of ZnS).

The excitonic effects are responsible for the difference between the calculated imaginary part of dielectric function and experiment in energy region close to the band gap. Exciton contributions to optical spectra of pure ZnS have not been included in this work. Excitonic absorption is clearly observed in a direct gap pure semiconductor in the spectral region close to the band gap [22]. A description of excitons requires a treatment of electron correlation beyond the GGA and LDA.

5.5 The Influence of Impurities on Optical Properties

Figures (5.40) and (5.41) show the calculated real and imaginary components of the frequency dependent dielectric function of $ZnMnS_2$ and $ZnCrS_2$ respectively. Here, the low-frequency limit of dielectric function deserves special attention, because impurity atoms introduce energy levels in the lower energy region within the band gap. As we have seen in Figure 5.38 the imaginary part of dielectric function is zero for pure ZnS at excitation energies less than the band gap (below 2.22 eV) while the real part of the dielectric function tends to be nearly constant.

Our results show that the real and imaginary part of the dielectric function change significantly in the lower frequency region (for the energy range less than the fundamental gap) after Mn and Cr impurities are incorporated into ZnS. In the higher energy region (above 10 eV) the absorption is quite similar for pure ZnS and impurity substituted ZnS.

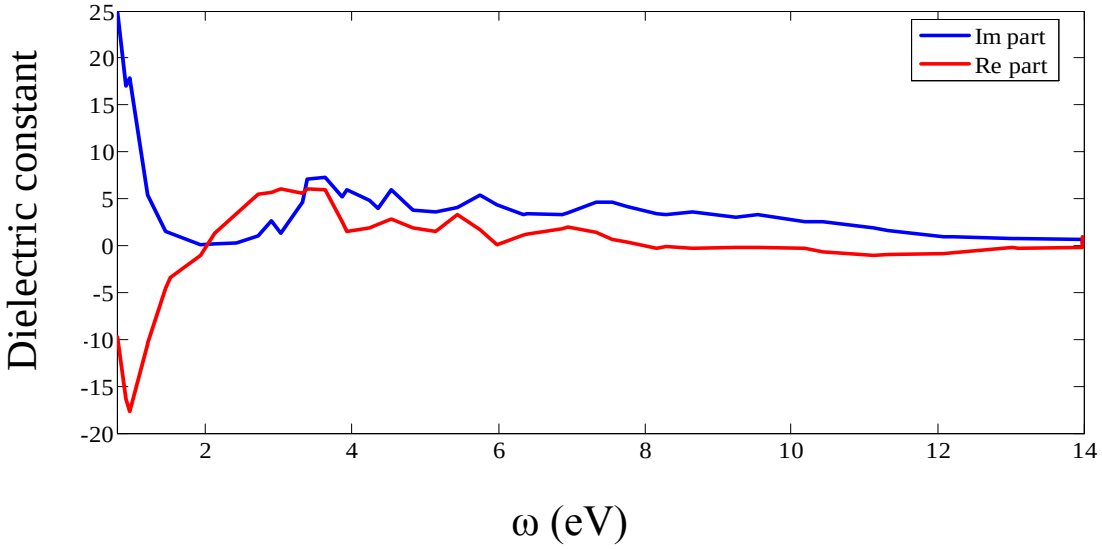

Figure 5.40: The calculated dielectric function of $ZnMnS_2$.

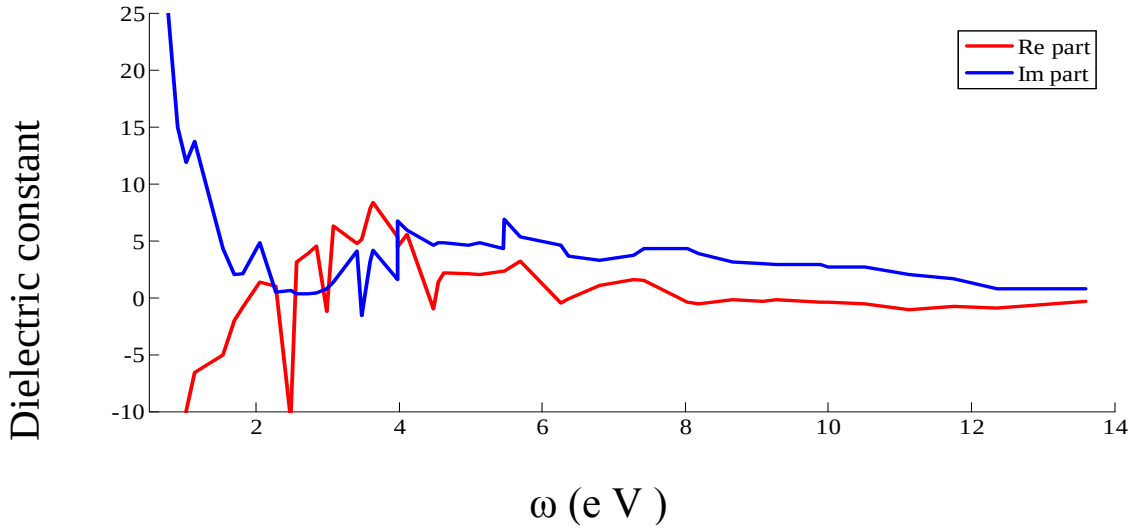

Figure 5.41: The calculated dielectric function of $ZnCrS_2$.

6. SUMMARY

We have presented density functional theory calculations of electronic and optical properties of ZnS, MnS, CrS, and effects of Mn and Cr impurities on electronic properties of pure ZnS using the periodic program BAND. In our calculations, we have used the generalized gradient approximation (GGA) of PW91 to approximate the exchange and correlation energies. The calculated electronic band structure results show that zinc-blende ZnS is a direct band gap material. The calculated electronic band structure and DOS results are in good agreement with previous theoretical and experimental results. Our results indicate that zinc-blende CrS shows a half-metallic behavior, while MnS shows semiconducting behavior.

Mn and Cr impurity substitution for Zn result in an expansion of the ZnS crystal structure and creates bulk defect states within the band gap. Mn impurities mainly affect the deep valence bands and the shallow conduction bands of ZnS. Cr impurities mainly affect the shallow and the deep valence bands. Our results for band structure and DOS show that a half-metallic behavior is found in Cr substituted ZnS while semiconducting behavior is found in Mn substituted ZnS.
Finally, the frequency dependent dielectric function was calculated to study optical properties. Our results for the dielectric function show that strong and direct absorption at the sharp peak in the spectral region around 6.05 eV is due to a high density of states at the X-point within the Brillouin zone. The calculated results showed intraband absorption in the low frequency region within the band gap, due to Mn and Cr impurity levels.

6.1 Future work

Results, discussion, and computational details used in this project give us the chance to mention some recommendations for future work.

Because of technological applications related to spintronics and magnetism, further investigation of half- metallic CrS is necessary to understand the origin of magnetism and electronic structure in detail. Different approach is required to solve integrals in *k* space for metallic MnS.

Further investigations on the influence of low doping fractions of Mn and Cr impurities on electronic, optical, and magnetic properties of ZnS are necessary to understand the technological applications related to solar cells and laser devices.

In this project, due to time limitation, it was mainly focused on studying effects of incorporation of Mn and Cr impurities at higher level of concentration on optical properties of pure ZnS. It is therefore necessary to study and understand the influence of Mn and Cr impurities on optical properties of ZnS for the lower doping concentrations.

The last step in improving this project would be to study electronic, magnetic, and optical properties of other transition metal impurities in zinc chalcogenides.

REFERENCES

[1] D.S. Sholl, J.A. Steckel, *Density functional theory: a practical introduction*, John Wiley & Sons, Inc, Hoboken, New Jersey, (2009).

[2] P. Hohenberg and W. Kohn, *Inhomogeneous electronic gas*, Phys. Rev. 136, B864, Nov (1964).

[3] F.Kootstra, *Time-Dependent Density Functional Theory For Periodi systems*, PhD Thesis, Groningen, The Netherlands, (2001).

[4] http://www.scm.com/Products/Overview/BANDInfo.html.

[5] http://www.scm.com/Products/Overview/ADFinfo.html.

[6] R. A. de Groot, F. M. Muller, P. G. van Engen, and K. H. J. Buschow, *New class of materials: Half-Metallic Ferromagnets*, Phys. Rev. Lett. **50**, 2024 (1983).

[7] K. Schwarzt, *CrO_2 predicted as a half-metallic ferromagnets*, J. Phys. F: Met. Phys. 16 (1986) L211-L215.

[8] H. Shoren, F. Ikemoto, K. Yoshida, N. Tanaka, K. Motizuki, *First principles electronic band calculation of (Zn, Cr)Te, (Zn, Cr)Se and (Zn, Cr)S*, Physica E 10 (2001) 242-246.

[9] Leach, A. R. Molecular Modelling: *Principles and Applications*, 2nd ed.; Prentice Hall: Upper Saddle River, New Jersey, (2001).

[10] A. C. Philips, *Introduction to Quantum Mechanics*, Jonh Wiley & Sons Ltd, Chichester, England, (2003).

[11] J.J. Sakuria, *Modern Quantum Mechanics*, Addison-Wesely Publishing Company, Inc, United States of America, (1994).

[12] K.L. Nielsen, *Theoretical studied of adsorption of atoms and small molecules on an oxygen terminated (0001) surfaces of alpha- chromium oxide*, NTNU Norges teknisk-naturvitenskapelige universitet, Trondheim, May 2008.

[13] J. Singh, *Smart Electronic Materials: Fundamentals and Applications*, Cambridge university press, United Kingdom, (2005).

[14] W. Kohn, A.D. Becke, and R.G. Parr, *Density Functional Theory of electronic structure*, J. Phys. Chem.100 (31), (1996).

[15] E.K.U Gross and Reiner M. Dreizler, *Density Functional Theory*, Plenum Press, New York, (1995).

[16] W. Kohn and L. J. Sham, Phys. Rev. 140 (4A), A1133–A1138, Nov (1965).

[17] E. Engel, R.M. Dreizler, *Density Functional Theory: An Advanced Course Series: Theoretical and Mathematical Physics*, 1st Edition, Springer-Verlag Berlin Heidelberg, (2011).

[18] R.G. Parr and W. Yang, *Density functional theory of atoms and molecules*, Oxford University Press, New York, 1989.

[19] E. Runge and E.K.U. Gross, Phys. Rev. Lett. **52**, 997 (1984).

[20] A. Thilagam, D. J. Simpson and A .R. Gerson, *A first-principles study of the dielectric properties of TiO_2 polymorphs*, J. Phys. Condens. Matter 23 (2011) 025901.

[21] F. Kootstra, P.L. de Boeij, and J.G. Snijders, *Application of time-dependent density-functional theory to the dielectric function of various nonmetallic crystals*, Physical Review B **62**, 7071 (2000).

[22] M. Fox, *Optical properties of solids*, second edition, Oxford University Press, Oxford, (2010).

[23] S. Botti, F. Sottile, N. Vast, V. Olevano, and L. Reining, *Long-range contribution to the exchange-correlation kernel of time-dependent density functional theory*, Phys. Rev. B 69, 155112 (2004).

[24] S. Nakajima, Y. Toyozawa, R. Abe, *The physics of elementary excitations*, Springer-Verlag, Berlin , Heidelberg, New York, (1980).

[25] M.L. Cohen and J.R.Chelikowsky, *Electronic structure and optical properties of semiconductors*, second edition, Springer-Verlag Berlin, (1989).

[26] F. Bassani, G. Pastori Parravicini, *Electronic states and optical transitions in solids*, Pergamon Press, Oxford, (1975).

[27] S. Kal, *Basic Electronics: Devices, Circuits and IT Fundamentals*, Prentice-Hall of India, New Delhi, (2003).

[28] *Numerical Data and Functional Relationships in Science and Technology* , edited by O. Madelung, Landolt-Bornstein, New Series, Vol 17b, Springer-Verlag, Berlin, (1982).

[29] C. Kittel, *Introduction to solid state physics,* eighth edition, John Wiley & Sons, Inc, United States of America, (2005).

[30] J.P. Perdew, J.A. Chevary, S.H. Vosko, K.A. Jackson, M.R. Pederson, D.J. Singh, and C.F Fiolhais, *Atoms, molecules, solids and surfaces: applications of the generalized gradient approximation for exchange and correlation*, Phys. Rev. B **46**, 6671(1992).

[31] G. te Velde and E. J. Baerends, *Precise density-functional method for periodic structures*, Phys. Rev. B **44**, 7888 (1991).

[32] H.J. Monkhorst and J.D. Pack, *Special Points for Brillouin zone integration*s, Phys. Rev. B **13**, 5188 (1976).

[33] P.E. Blochl, O. Jepsen, and O.K. Andersen, *Improved tetrahedron method for Brillouin-zone integrations*, Phys. Rev. B **49**, 16223 (1994).

[34] K.N. Nigussa, *Density functional theory investigations of surface structure and reactivity*, PhD Thesis, NTNU Norges teknisk-naturvitenskapelige universitet, Trondheim, (2011).

[35] J. E. Jaffe, R. Pandey, and M. J. Seel, *Ab initio high-pressure structural and electronic properties of ZnS*, Phys. Rev. B47, 11 (1992).

[36] M. Bilge, S. Ozdemir Kart, H.H Kart, T. Cagin, *Mechanical and electronical properties of ZnS under pressure*, Volume 31 (2008).

[37] K. L.Yao, G. Y. Gao, Z. L. Liu, L. Zhu, *Half-metallic ferromagnetism of Zinc-blende CrS and CrP: a first-principles pseudopotential study*, solid state communication 133 (2005) 301-304.

[38] R. Khenata, A. Bouhemadou, M. Sahnoun, A.H. Reshak, H. Baltache, M. Rabah, *Elastic, electronic and optical properties of ZnS, ZnSe and ZnTe under pressure*, Computational Materials Science, 38 (2006) 29-38.